Journal of Computational Mathematics
Vol.xx, No.x, 2025, 1–31.

http://www.global-sci.org/jcm
doi:10.4208/jcm.2509-m2024-0165

LOW-DEGREE $\mathcal{O}(h^2)$-ACCURATE CONSERVATIVE FINITE ELEMENT SCHEMES FOR INCOMPRESSIBLE STOKES PROBLEMS ON GENERAL TRIANGULATIONS*

Wenjia Liu
School of Mathematics and Statistics, Shanxi University, Taiyuan 030006, China
Email: wjliu@sxu.edu.cn
Huilan Zeng
Tsinghua University High School, Beijing 100084, China
Email: zhl@lsec.cc.ac.cn
Shuo Zhang[1)]
State Key Laboratory of Mathematical Sciences and State Key Laboratory of Scientific and Engineering Computing,
Institute of Computational Mathematics and Scientific/Engineering Computing,
Academy of Mathematics and Systems Science, Chinese Academy of Sciences,
Beijing 100190, China;
School of Mathematical Sciences, University of Chinese Academy of Sciences,
Beijing 100049, China
Email: szhang@lsec.cc.ac.cn

Abstract

In this paper, two $\mathcal{O}(h^2)$-accurate conservative finite element schemes with low-degree polynomials for the incompressible Stokes equations are presented. The schemes use respective $H(\mathrm{div})$ finite element spaces, namely the third-order Brezzi-Douglas-Marini space and Brezzi-Douglas-Fortin-Marini space, with enhanced smoothness for the velocity and piecewise quadratic polynomials for the pressure, and are denoted as $\mathrm{sBDM}_3 - \mathrm{P}_2$ and $\mathrm{sBDFM}_3 - \mathrm{P}_2$ schemes, respectively. The discrete Korn inequality holds for both sBDM_3 and sBDFM_3 finite element spaces. For the $\mathrm{sBDM}_3 - \mathrm{P}_2$ scheme, the inf-sup condition holds on general triangulations, and for the $\mathrm{sBDFM}_3 - \mathrm{P}_2$ scheme, the inf-sup condition holds on triangulations with mild restriction. Both schemes achieve an energy norm of velocity errors of $\mathcal{O}(h^2)$ order and an L^2-norm of pressure errors of $\mathcal{O}(h^2)$ order. Numerical experiments support the theoretical constructions.

Mathematics subject classification: 65N12, 65N30, 76D05.
Key words: Stokes equations, Strictly conservative finite element, Low-degree, $\mathcal{O}(h^2)$-accurate, inf-sup stability.

1. Introduction

The incompressible Stokes problem is a fundamental model problem. Its divergence constraint $\mathrm{div}\boldsymbol{u} = 0$ represents the incompressibility of the fluid, or equivalently the conservation of mass, and separates the velocity independently from pressure. If a stable finite element scheme is

* Received August 4, 2024 / Revised version received September 23, 2025 / Accepted September 26, 2025 / Published online December 26, 2025 /
1) Corresponding author

pressure-robust or conservative, i.e., it strictly maintains the divergence constraint and inherits mass conservation, then the approximation of the velocity can be independent of the pressure as exhibited in the continuous equations, and the method does not suffer from the locking effect with respect to a high Reynolds number [3]. The strict conservation is also of crucial importance in, e.g., the nonlinear mechanics [1,2] and the magnetohydrodynamics [11–13]. Designing conservative schemes has attracted much research interest.

Many approaches have been developed to construct conservative schemes. Following [14], they can roughly be divided into three categories: mixed Galerkin schemes constructed by the de Rham complex [6,10], $\boldsymbol{H}(\mathrm{div})$-conforming schemes [5,9,15,22,24,25,27], and indirect methods including the grad-div stablization [7,8] and appropriate reconstructions of test functions [16,17] and so on. Conservative schemes of $\mathcal{O}(h)$-accuracy have been well studied in [9,19,22,27] where cubic or higher-degree polynomials are adopted for velocity approximation. Recently, [18,29] presented $\boldsymbol{H}(\mathrm{div})$-conforming finite element pairs which are stable and conservative on general triangulations. All the pairs of [18,29] fall into the second category($\boldsymbol{H}(\mathrm{div})$-conforming schemes). Though, different from the known methods(e.g., [9,22,27]) whose idea is to add some bubble functions to a simple $\boldsymbol{H}(\mathrm{div})$-conforming space to enhance weak tangential continuity, the tactic in [18,29] is to impose weak tangential continuity upon the well-known Brezzi-Douglas-Marini (BDM) and Brezzi-Douglas-Fortin-Marini (BDFM) finite element spaces. Some low-degree finite element pairs are given in [18,29], and particularly, a $\mathbf{P}^{1+}-\mathrm{P}_0$ scheme given in [18], which adopts a slightly enriched piecewise linear polynomial space for the velocity, is demonstrated to be of the theoretically lowest-degree on general triangulations.

In this paper, we present two stable and conservative schemes of $\mathcal{O}(h^2)$-accuracy with low-degree polynomials locally. The construction of high-order and low-degree schemes pursues a high balance between computational accuracy and efficiency. Some $\mathcal{O}(h^2)$-accurate conservative schemes have been studied in, e.g., [9,10,27], where the polynomials with fourth and higher degrees are adopted. Lower-degree $\mathcal{O}(h^2)$-accurate conservative schemes can be found in [20], but an essentially restrictive assumption is needed for the triangulation. Motivated by [18,29], in this paper, we construct so-called sBDM_3 and sBDFM_3 spaces by enhancing the third order BDM and BDFM finite element spaces with weak tangential continuity to obtain new $\boldsymbol{H}(\mathrm{div})$-conforming spaces. The discrete Korn inequality holds for both sBDM_3 and sBDFM_3 finite element spaces. The $\mathrm{sBDM}_3-\mathrm{P}_2$ and $\mathrm{sBDFM}_3-\mathrm{P}_2$ schemes achieve an $\mathcal{O}(h^2)$ convergence order in the energy norm, and as far as we know, they are of the lowest-degree among the $\mathcal{O}(h^2)$-accurate schemes up to date on general triangulations and on mildly restricted triangulations respectively. The main technical ingredients of this article are inf-sup conditions established for the two finite element space pairs. We adopt Stenberg's macroelement technique to show both of them. Particularly, the inf-sup condition holds for $\mathrm{sBDM}_3-\mathrm{P}_2$ scheme on general triangulations, and for $\mathrm{sBDFM}_3-\mathrm{P}_2$ scheme on triangulations under some restrictions, which are mild and can be satisfied by, e.g., the frequently used well-centered grids [23]. Numerical experiments verify the theoretical results. Further, it can be observed that the stability of the $\mathrm{sBDFM}_3-\mathrm{P}_2$ scheme seems not sensitive to the triangulation, and, for Stokes eigenvalue problems, the computed eigenvalues may tend to the exact ones monotonously when the mesh is fine enough.

The remainder of the paper is organized as follows. Section 2 consists of fundamental notations, the basic theory of the Stokes equations and a review of Stenberg's macroelement technique. Section 3 contains the main results of this paper, including two novel finite element schemes, the $\mathrm{sBDM}_3-\mathrm{P}_2$ and the $\mathrm{sBDFM}_3-\mathrm{P}_2$, their corresponding theoretical construction, and numeri-

cal performance. For the readers' ease, we postpone the technical proofs of Lemmas 3.1 and 3.3 to Sections 4 and 5 respectively, and the readers will not be involved into details in Section 3. Appendix A exhibits more detailed proofs of certain lemmas in Sections 4 and 5.

2. Preliminary

2.1. Notations

In this paper, we use Ω to denote a simply connected polygonal domain. We use $H^1(\Omega)$, $H_0^1(\Omega), H^2(\Omega), \boldsymbol{H}(\mathrm{div},\Omega)$ and $L^2(\Omega)$ to denote certain Sobolev spaces, and denote

$$L_0^2(\Omega) := \left\{ w \in L^2(\Omega) : \int_\Omega w dx = 0 \right\}.$$

We use a letter in boldface to denote a vector-valued function or function space. Particularly, $\boldsymbol{H}_0^1(\Omega) := (H_0^1(\Omega))^2$. The gradient and divergence operators are denoted by ∇ and div respectively. Let $\mathcal{T}_h$ be a shape-regular triangular subdivision of Ω such that $\overline{\Omega} = \cup_{T\in\mathcal{T}_h}\overline{T}$. We use the subscript "$\cdot_h$" to denote the dependence on triangulation. In particular, an operator with the subscript "$\cdot_h$" indicates that the operation is performed cell by cell. In addition, $\|\cdot\|_{1,h}$ denotes the mesh-dependent $\boldsymbol{H}^1$-norm

$$\|\boldsymbol{v}\|_{1,h}^2 := \sum_{T\in\mathcal{T}_h} \|\boldsymbol{v}\|_{1,T}^2.$$

A generic constant C throughout this paper depends on the domain, and when triangulation is involved, it also depends on the shape regularity of the triangulation, but not on h or any other mesh parameter.

Denote $\mathcal{X}_h, \mathcal{X}_h^i, \mathcal{X}_h^b, \mathcal{E}_h, \mathcal{E}_h^i$ and $\mathcal{E}_h^b$ as the set of vertices, interior vertices, boundary vertices, edges, interior edges, and boundary edges, respectively. For any edge $e \in \mathcal{E}_h$, denote $\boldsymbol{n}_e$ and $\boldsymbol{t}_e$ as the globally defined unit normal and tangential vectors of e, respectively. The subscript $\cdot_e$ can be dropped when there is no ambiguity. In addition, τ denotes the arc length along e.

On the triangle T with vertices $\{a_1, a_2, a_3\}$ and edges $\{e_1, e_2, e_3\}$, we denote local unit outward normal vectors by $\{\boldsymbol{n}_1, \boldsymbol{n}_2, \boldsymbol{n}_3\}$ and local unit tangential vectors $\{\boldsymbol{t}_1, \boldsymbol{t}_2, \boldsymbol{t}_3\}$ such that $\boldsymbol{n}_i \times \boldsymbol{t}_i > 0$, $i \in \{1,2,3\}$; see Fig. 2.1 for an illustration. In addition $\{\lambda_1, \lambda_2, \lambda_3\}$ are the barycentric coordinates with respect to the three vertexes of T. And $\{l_1, l_2, l_3\}$ are the lengths of $\{e_1, e_2, e_3\}$.

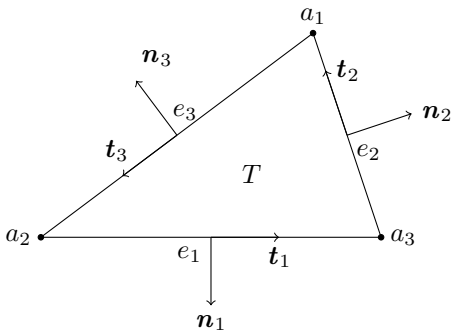

Fig. 2.1. A triangle.

Also, we denote the area of T as S_T, and we drop the subscript when no ambiguity exists. Specifically, S_{T_i} shall be written as S_i. Moreover, we use $P_k(T)$ and $P_k(e)$ respectively to denote the set of polynomials on the T and e of degrees not higher than k. Also, $\boldsymbol{P}_k(T) := (P_k(T))^2$, $\boldsymbol{P}_k(e) := (P_k(e))^2$.

Let h_T and ρ_T be the circumradius and inradius of T, respectively. Let $h := \max_{T\in\mathcal{T}_h} h_T$ be the mesh size of $\mathcal{T}_h$.

Assumption 2.1. We assume that $\mathcal{T}_h$ is a family of regular subdivisions, that is,

$$\max_{T\in\mathcal{T}_h} \frac{h_T}{\rho_T} \leqslant \gamma_0,$$

where γ_0 is a generic constant independent of h.

Assumption 2.2. Every boundary vertex is connected to at least one interior vertex.

2.2. Model problem

The incompressible Stokes problem is

$$\begin{cases} -\varepsilon^2 \Delta\, \boldsymbol{u} + \nabla\, p = \boldsymbol{f} & \text{in } \Omega, \\ \operatorname{div} \boldsymbol{u} = 0 & \text{in } \Omega, \\ \boldsymbol{u} = 0 & \text{on } \partial\Omega. \end{cases} \tag{2.1}$$

Here, $\boldsymbol{u}$ is the velocity field, p is the pressure field of the incompressible flow, and ε^2 is the inverse of the Reynolds number, which can be small. The variational formulation is to find $(\boldsymbol{u}, p) \in \boldsymbol{H}_0^1(\Omega) \times L_0^2(\Omega)$ such that

$$\begin{cases} a(\boldsymbol{u}, \boldsymbol{v}) + b(\boldsymbol{v}, p) = (f, \boldsymbol{v}), & \forall\, \boldsymbol{v} \in \boldsymbol{H}_0^1(\Omega), \\ b(\boldsymbol{u}, q) = 0, & \forall\, q \in L_0^2(\Omega), \end{cases} \tag{2.2}$$

where

$$a(\boldsymbol{v}, \boldsymbol{v}) := \varepsilon^2(\nabla\, \boldsymbol{u}, \nabla\, \boldsymbol{v}), \quad b(\boldsymbol{v}, q) := -(\operatorname{div} \boldsymbol{v}, p).$$

Let $\boldsymbol{V}_h$ and Q_h be two finite element spaces to approximate $\boldsymbol{H}_0^1(\Omega)$ and $L_0^2(\Omega)$ respectively, and consider the following discrete variational form: Find $(\boldsymbol{u}_h, p_h) \in \boldsymbol{V}_h \times Q_h$ such that

$$\begin{cases} a_h(\boldsymbol{u}_h, \boldsymbol{v}_h) + b_h(\boldsymbol{v}_h, p_h) = (f, \boldsymbol{v}_h), & \forall\, \boldsymbol{v}_h \in \boldsymbol{V}_h, \\ b_h(\boldsymbol{u}_h, q_h) = 0, & \forall\, q_h \in Q_h, \end{cases} \tag{2.3}$$

where

$$a_h(\boldsymbol{u}_h, \boldsymbol{v}_h) := \sum_{T\in\mathcal{T}_h} \int_T \nabla \boldsymbol{u}_h \cdot \nabla \boldsymbol{v}_h \,\mathrm{d}\boldsymbol{x},$$

$$b_h(\boldsymbol{u}_h, q_h) := -\sum_{T\in\mathcal{T}_h} \int_T \operatorname{div} \boldsymbol{u}_h \, q_h \,\mathrm{d}\boldsymbol{x}.$$

2.3. Stenberg's macroelement technique for inf-sup condition [21]

A macroelement is a connected set of at least two cells in $\mathcal{T}_h$. A macroelement partition of $\mathcal{T}_h$, denoted by $\mathcal{M}_h$, is a set of macroelements satisfying that each triangle of $\mathcal{T}_h$ is covered by at least one macroelement in $\mathcal{M}_h$.

Definition 2.1. *Two macroelements M_1 and M_2 are said to be equivalent if there exists a continuous one-to-one mapping $G : M_1 \to M_2$ such that*

(a) $G(M_1) = M_2$.

(b) If $M_1 = \bigcup_{i=1:m}^{m} T_i^1$, *then* $T_i^2 = G(T_i^1)$ *with* $i = 1 : m$ *are the cells of* M_2.

(c) $G|_{T_i^1} = F_{T_i^2} \circ F_{T_i^1}^{-1}, i = 1 : m$, *where* $F_{T_i^1}$ *and* $F_{T_i^2}$ *are the mappings from a reference element* $\hat{T}$ *onto* T_i^1 *and* T_i^2, *respectively.*

A class of equivalent macroelements is a set of macroelements such that any two are equivalent to each other. Given a macroelement M, $\boldsymbol{V}_{h0,M}$, a subspace of $\boldsymbol{V}_h$, consists of functions in $\boldsymbol{V}_h$ that are equal to zero outside M; and continuity constraints of $\boldsymbol{V}_h$ enable corresponding nodal parameters of functions in $\boldsymbol{V}_{h0,M}$ to be zero on ∂M. Similarly, $Q_{h,M}$ is a subspace of Q_h and it consists of functions that are equal to zero outside M. Denote

$$N_M := \left\{ q_h \in Q_{h,M} : \int_M \operatorname{div} \boldsymbol{v}_h \, q_h \, dM = 0, \ \forall \, \boldsymbol{v}_h \in \boldsymbol{V}_{h0,M} \right\}. \tag{2.4}$$

Stenberg's macroelement technique in [21] can be summarized as the following proposition.

Proposition 2.1. *Suppose there exists a macroelement partitioning $\mathcal{M}_h$ with a fixed set of equivalence classes $\mathbb{E}_i$ of macroelements, $i = 1, 2, \ldots, n$, a positive integer N (n and N are independent of h), and an operator $\Pi : H_0^1(\Omega) \to \boldsymbol{V}_{h0}$ such that*

(C_1) For each $M \in \mathbb{E}_i, i = 1, 2, \ldots, n$, the space N_M defined in (2.4) is one-dimensional and it only consists of the functions which are constant on M.

(C_2) Each $M \in \mathcal{M}_h$ belongs to one of the classes $\mathbb{E}_i, i = 1, 2, \ldots, n$.

(C_3) Each $e \in \mathcal{E}_h^i$ is an interior edge of at least one and no more than N macroelements.

(C_4) For any $\boldsymbol{w} \in \boldsymbol{H}_0^1(\Omega)$, it holds that

$$\sum_{T \in \mathcal{T}_h} h_T^{-2} \|\boldsymbol{w} - \Pi \boldsymbol{w}\|_{0,T}^2 + \sum_{e \in \mathcal{E}_h^i} h_e^{-1} \|\boldsymbol{w} - \Pi \boldsymbol{w}\|_{0,e}^2 \leqslant C \|\boldsymbol{w}\|_{1,\Omega}^2, \quad \|\Pi \boldsymbol{w}\|_{1,h} \leqslant C \|\boldsymbol{w}\|_{1,\Omega}.$$

Then the uniform inf-sup condition holds for the finite element pair.

3. Main Results of This Paper

3.1. A conservative finite element scheme with $\mathcal{O}(h^2)$ accuracy on general grids

3.1.1. A smoothened Brezzi-Douglas-Marini finite element space

An sBDM$_3$ finite element is defined by the following triple $(T, \boldsymbol{P}_T, \boldsymbol{D}_T)$:

(1) T is a triangle.

(2) $\boldsymbol{P}_T = \boldsymbol{P}_3(T)$.

(3) For any $\boldsymbol{v} \in \boldsymbol{H}^1(T)$, the nodal parameters on T, denoted by $\boldsymbol{D}_T$, are

- $\fint_e (\boldsymbol{v}\cdot\boldsymbol{n})\tau^k \mathrm{d}\tau$, $k = 0,1,2,3$, $e \in \{e_1, e_2, e_3\}$;
- $\fint_e (\boldsymbol{v}\cdot\boldsymbol{t})\tau^k \,\mathrm{d}\tau$, $k = 0,1$, $e \in \{e_1, e_2, e_3\}$;
- $\fint_T \boldsymbol{v}^{(1)} \,\mathrm{d}x\mathrm{d}y$, $\fint_T \boldsymbol{v}^{(2)} \,\mathrm{d}x\mathrm{d}y$.

Elementary calculation shows that $\boldsymbol{D}_T$ is $\boldsymbol{P}_T$-unisolvent, and a set of nodal basis functions is admitted. For a specific choice of the degrees of freedom, please refer to the first column of Table 4.1.

Define sBDM$_3$ finite element spaces as follows:

$$\boldsymbol{V}_h^{\mathrm{sBDM}_3} := \Big\{ \boldsymbol{v}_h \in \boldsymbol{H}(\mathrm{div},\Omega) : \boldsymbol{v}_h|_T \in \boldsymbol{P}_3(T),\ \forall\, T \in \mathcal{T}_h; \\ \fint_e (\boldsymbol{v}_h\cdot\boldsymbol{t})\tau^k \mathrm{d}\tau\ (k=0,1)\ \text{are continuous across interior edges}\ e \in \mathcal{E}_h^i \Big\}, \tag{3.1}$$

$$\boldsymbol{V}_{h0}^{\mathrm{sBDM}_3} := \Big\{ \boldsymbol{v}_h \in \boldsymbol{V}_h^{\mathrm{sBDM}_3} : \boldsymbol{v}_h\cdot\boldsymbol{n} = 0 \ \text{ and } \ \fint_e (\boldsymbol{v}_h\cdot\boldsymbol{t})\tau^k \mathrm{d}\tau = 0\ (k=0,1),\ \forall\, e \in \mathcal{E}_h^b \Big\}. \tag{3.2}$$

By definition, $\boldsymbol{V}_h^{\mathrm{sBDM}_3} \subset H(\mathrm{div},\Omega)$ but $\boldsymbol{V}_h^{\mathrm{sBDM}_3} \not\subset \boldsymbol{H}^1(\Omega)$, and similarly $\boldsymbol{V}_{h0}^{\mathrm{sBDM}_3} \subset H(\mathrm{div},\Omega)$ but $\boldsymbol{V}_{h0}^{\mathrm{sBDM}_3} \not\subset \boldsymbol{H}^1(\Omega)$. Also, it holds that both $\boldsymbol{V}_h^{\mathrm{sBDM}_3}$ and $\boldsymbol{V}_{h0}^{\mathrm{sBDM}_3}$ are smoothened subspaces of the third-order BDM finite element spaces with weak tangential continuity.

We define a nodal interpolation operator $\Pi_h : \boldsymbol{H}^1(\Omega) \to \boldsymbol{V}_h^{\mathrm{sBDM}_3}$ such that for any $e \subset \mathcal{E}_h$,

$$\fint_e (\Pi_h\boldsymbol{v}\cdot\boldsymbol{n})\tau^k \mathrm{d}\tau = \fint_e (\boldsymbol{v}\cdot\boldsymbol{n})\tau^k \mathrm{d}\tau, \quad k = 0,1,2,3,$$
$$\fint_e (\Pi_h\boldsymbol{v}\cdot\boldsymbol{t})\tau^k \mathrm{d}\tau = \fint_e (\boldsymbol{v}\cdot\boldsymbol{t})\tau^k \mathrm{d}\tau, \quad k = 0,1.$$

The operator is locally defined on each triangle, and is invariant under Piola's transformation. Moreover, Π_h preserves cubic polynomials locally. Therefore, approximation estimates of Π_h can be derived from [3, Lemma 2.1.5, Remark 2.1.8], along with standard scaling arguments and the Bramble-Hilbert lemma.

Proposition 3.1. *It holds for* $0 \le k \le 1 \le s \le 3$ *that*

$$|\boldsymbol{v} - \Pi_h\boldsymbol{v}|_{k,h} \lesssim h^{s-k}\,|\boldsymbol{v}|_{s,\Omega}, \quad \forall\, \boldsymbol{v} \in \boldsymbol{H}^s(\Omega). \tag{3.3}$$

3.1.2. Theoretical constructions of the scheme

Now we define a couple of specific Q_h as follows:

$$Q_h^2 := \big\{ q_h \in L^2(\Omega) : q_h|_T \in P_2(T), \forall\, T \in \mathcal{T}_h \big\}, \quad Q_{h*}^2 := Q_h^2 \cap L_0^2(\Omega), \tag{3.4}$$

and consider the finite element discretization: Find $(\boldsymbol{u}_h, p_h) \in \boldsymbol{V}_{h0}^{\mathrm{sBDM}_3} \times Q_{h*}^2$ such that

$$\begin{cases} \varepsilon^2(\nabla_h \boldsymbol{u}_h, \nabla_h \boldsymbol{v}_h) - (\mathrm{div}\boldsymbol{v}_h, p_h) = (\boldsymbol{f}, \boldsymbol{v}_h), & \forall\, \boldsymbol{v}_h \in \boldsymbol{V}_{h0}^{\mathrm{sBDM}_3}, \\ (\mathrm{div}\boldsymbol{u}_h, q_h) = 0, & \forall\, q_h \in Q_{h*}^2. \end{cases} \tag{3.5}$$

The corresponding finite element scheme is denoted by $\mathrm{sBDM}_3 - \mathrm{P}_2$.

Lemma 3.1 (Stability of $\boldsymbol{V}_{h0}^{\mathrm{sBDM}_3} \times Q_{h*}^2$). *Let $\mathcal{T}_h$ be a family of triangulations of Ω satisfying Assumptions* 2.1 *and* 2.2. *Then it holds that*

$$\inf_{q_h \in Q_{h*}^2} \sup_{\boldsymbol{v}_h \in \boldsymbol{V}_{h0}^{\mathrm{sBDM}_3}} \frac{(\mathrm{div}\boldsymbol{v}_h, q_h)}{\|q_h\|_{0,\Omega}\|\boldsymbol{v}_h\|_{1,h}} \geqslant C > 0. \tag{3.6}$$

The proof of Lemma 3.1 is a combination of Proposition 2.1, Lemmas 4.1-4.3 and please refer to Section 4 for more details.

By the tangential continuity of $\boldsymbol{V}_{h0}^{\mathrm{sBDM}_3}$, the following discrete Korn inequality holds [26].

Lemma 3.2 (Discrete Korn Inequality). *Denote $\epsilon(\boldsymbol{u}) := (\nabla \boldsymbol{u} + (\nabla \boldsymbol{u})^\top)/2$. Then*

$$\|\boldsymbol{u}\|_{1,h}^2 \leqslant C \sum_{T \in \mathcal{T}_h} \|\epsilon(\boldsymbol{u})\|_{0,T}^2, \quad \forall\, \boldsymbol{u} \in \boldsymbol{V}_{h0}^{\mathrm{sBDM}_3}. \tag{3.7}$$

It is evident that (3.5) is a stable and conservative discretization scheme and its well-posedness is immediate. By standard theory, the theorem below holds.

Theorem 3.1. *Let $(\boldsymbol{u}, p)$ and $(\boldsymbol{u}_h, p_h)$ be the solutions of* (2.2) *and* (3.5), *respectively. If $(\boldsymbol{u}, p) \in \boldsymbol{H}^3(\Omega) \times H^2(\Omega)$, then*

$$|\boldsymbol{u} - \boldsymbol{u}_h|_{1,h} \leqslant Ch^2|\boldsymbol{u}|_{3,\Omega}, \quad \|p - p_h\|_{0,\Omega} \leqslant Ch^2|p|_{2,\Omega} + C\varepsilon^2 h^2|\boldsymbol{u}|_{3,\Omega}.$$

3.1.3. Numerical experiments

In this subsubsection, we present two series of numerical examples about the $\mathrm{sBDM}_3 - \mathrm{P}_2$ finite element scheme. Example 3.1 is designed to validate the convergence theory in Theorem 3.1 and Example 3.2 to illustrate the numerical performance of $\mathrm{sBDM}_3 - \mathrm{P}_2$ for the Stokes eigenvalue problem (3.8). Each series of numerical examples are computed on the five domains, three of which are convex, and the other two of which are non-convex. Namely,

- Square (Fig. 3.1(a)). $A_1(0,0)$, $A_2(1,0)$, $A_3(1,1)$, $A_4(0,1)$;
- Hexagon (Fig. 3.1(b)). $A_1(0,0)$, $A_2(0.5,0)$, $A_3(1,0.5)$, $A_4(1,1)$, $A_5(0.5,1)$, $A_6(0,0.5)$;
- Pentagon (Fig. 3.1(c)). $A_1(-0.1,-0.8)$, $A_2(0.9,-0.15)$, $A_3(1,1)$, $A_4(-0.6,0.8)$, $A_5(-1,0)$;
- L-shape (Fig. 3.1(d)). $A_1(0,0)$, $A_2(2,0)$, $A_3(2,1)$, $A_4(1,1)$, $A_5(1,2)$, $A_6(0,2)$;
- Star-shape (Fig. 3.1(e)). $A_1(-1,-1.2)$, $A_2(-0.1,-0.8)$, $A_3(0.7,-1.1)$, $A_4(0.6,-0.3)$, $A_5(0.8,0.35)$, $A_6(0.4,0.4)$, $A_7(0,1.1)$, $A_8(-0.5,0.5)$, $A_9(-1.2,0.25)$, $A_{10}(-0.8,-0.3)$.

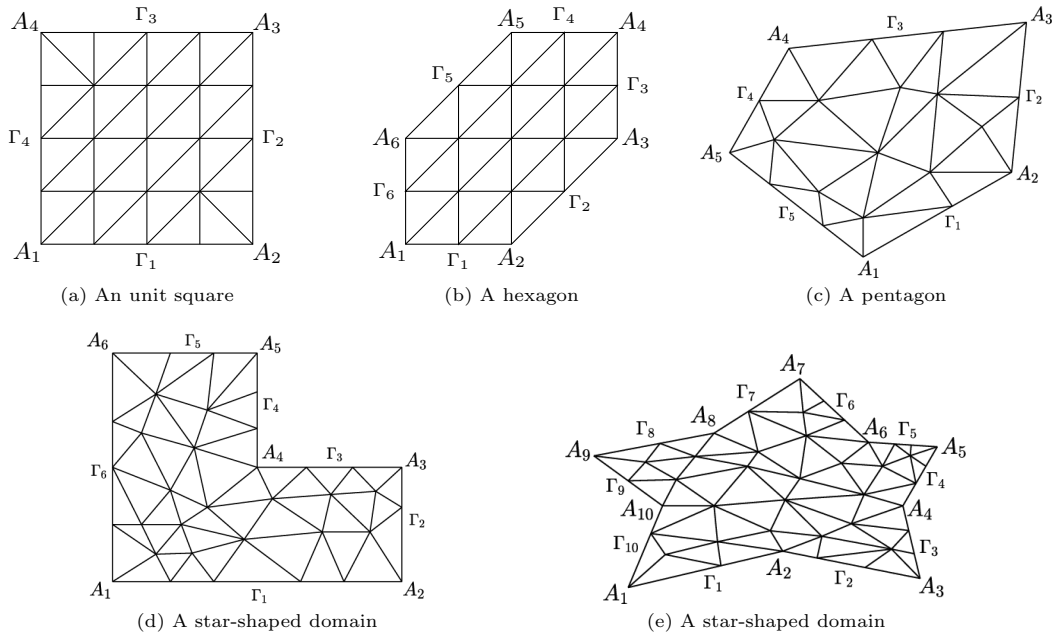

(a) An unit square (b) A hexagon (c) A pentagon

(d) A star-shaped domain (e) A star-shaped domain

Fig. 3.1. Five domains: three (the upper row) are convex, and two (the lower row) are non-convex.

Example 3.1. Consider the Stokes problem (2.1) in the five domains. For each domain, $\partial\Omega = \cup_i \Gamma_i$. Define

$$\phi = C_\phi \prod_{\Gamma_i \subset \partial\Omega} \big(r(\Gamma_i)\big)^2, \quad r(\Gamma_i) = 0$$

representing the equation of Γ_i. Assume $\varepsilon = 1$ and the right-hand side $\boldsymbol{f}$ is chosen such that the exact solution pair is $\boldsymbol{u} = \operatorname{curl}\phi$ and $p = 3x^2 + 3y^2 + C_p$ where p satisfies $\int_\Omega p\,dx = 0$.

Fig. 3.2 demonstrates that consistent with Theorem 3.1, the velocity errors in $\boldsymbol{H}^1$-norm are of $\mathcal{O}(h^2)$ order and $\boldsymbol{L}^2$-norm are of $\mathcal{O}(h^3)$ order; the pressure errors in L^2-norm are of $\mathcal{O}(h^2)$ order.

Example 3.2. The variational form of the Stokes eigenvalue problem is: find $(\boldsymbol{u}, p, \lambda) \in \boldsymbol{H}_0^1(\Omega) \times L_0^2(\Omega) \times \mathbb{R}$, such that

$$\begin{cases} (\nabla \boldsymbol{u}, \nabla \boldsymbol{v}) - (\operatorname{div}\boldsymbol{v}, p) = \lambda(\boldsymbol{u}, \boldsymbol{v}), & \forall\, \boldsymbol{v} \in \boldsymbol{H}_0^1(\Omega), \\ (\operatorname{div}\boldsymbol{u}, q) = 0, & \forall\, q \in L_0^2(\Omega). \end{cases} \tag{3.8}$$

Consider the discrete form of (3.8): find $(\boldsymbol{u}_h, p_h) \in \boldsymbol{V}_{h0}^{\mathrm{sBDM}_3} \times Q_{h*}^2$ and $\lambda \in \mathbb{R}$ such that

$$\begin{cases} (\nabla_h \boldsymbol{u}_h, \nabla_h \boldsymbol{v}_h) - (\operatorname{div}\boldsymbol{v}_h, p_h) = \lambda(\boldsymbol{u}_h, \boldsymbol{v}_h), & \forall\, \boldsymbol{v}_h \in \boldsymbol{V}_{h0}^{\mathrm{sBDM}_3}, \\ (\operatorname{div}\boldsymbol{u}_h, q_h) = 0, & \forall\, q_h \in Q_{h*}^2. \end{cases}$$

Simulations are performed on the five domains in Fig. 3.1 and six minimum eigenvalues are recorded. Denote, for an indication to the convergence rate,

$$\text{order} := \log_2\left(\frac{\lambda_{2h} - \lambda_{4h}}{\lambda_h - \lambda_{2h}}\right),$$

which is computed for each case and recorded in the Tables 3.1-3.5.

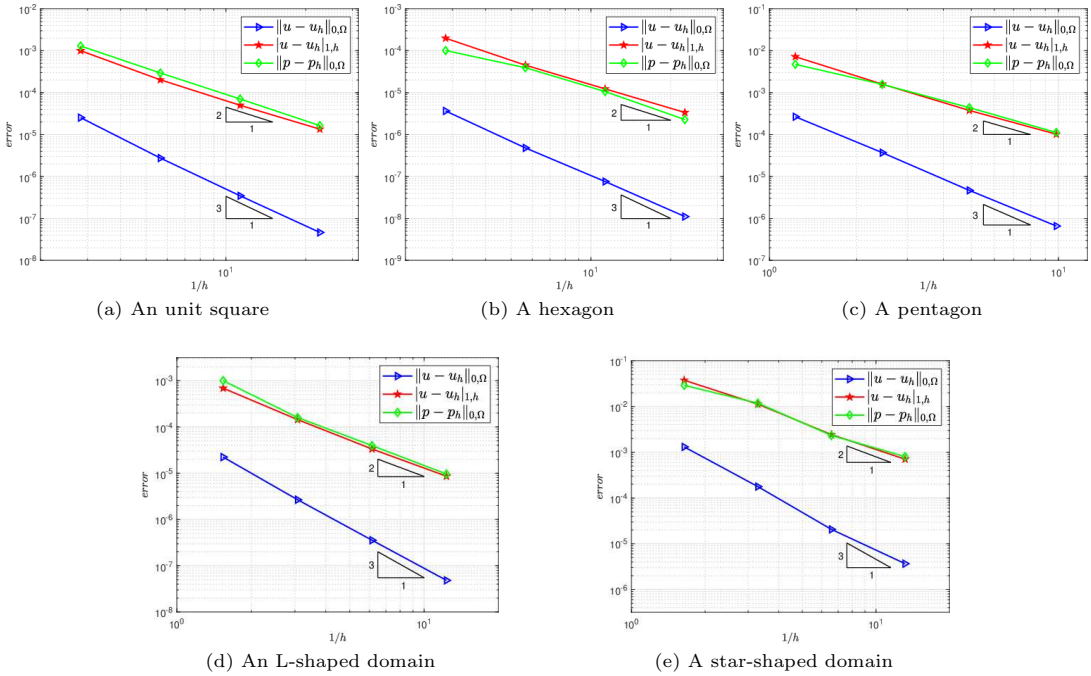

(a) An unit square (b) A hexagon (c) A pentagon

(d) An L-shaped domain (e) A star-shaped domain

Fig. 3.2. Velocity errors in the L^2- and H^1-norm and pressure errors in the L^2-norm by the $\mathrm{sBDM}_3 - \mathrm{P}_2$ pair on five domains.

Table 3.1: Six minimum eigenvalues computed on Fig. 3.1(a) by the $\mathrm{sBDM}_3 - \mathrm{P}_2$ pair.

Mesh	0	1	2	3	4	Trend	Order
$\lambda_{1,h}$	52.3651	52.3441	52.3446	52.3447	52.3447	↗	3.4261
$\lambda_{2,h}$	92.2727	92.1226	92.1239	92.1244	92.1244	↗	3.4026
$\lambda_{3,h}$	92.2817	92.1229	92.1239	92.1244	92.1244	↗	3.4115
$\lambda_{4,h}$	128.6782	128.2107	128.2087	128.2095	128.2096	↗	3.1054
$\lambda_{5,h}$	155.5963	154.1251	154.1233	154.1253	154.1254	↗	3.4502
$\lambda_{6,h}$	168.8246	167.0288	167.0265	167.0289	167.0292	↗	3.3876

Table 3.2: Six minimum eigenvalues computed on Fig. 3.1(b) by the $\mathrm{sBDM}_3 - \mathrm{P}_2$ pair.

Mesh	0	1	2	3	4	Trend	Order
$\lambda_{1,h}$	79.6035	80.6981	80.7412	80.7458	80.7461	↗	3.9166
$\lambda_{2,h}$	108.4275	102.6239	103.1018	103.1232	103.1247	↗	3.9468
$\lambda_{3,h}$	155.6664	150.3831	149.4039	149.4235	149.4263	↗	3.5410
$\lambda_{4,h}$	174.3579	169.6303	169.7040	169.7217	169.7234	↗	3.8338
$\lambda_{5,h}$	199.4150	198.1051	198.4128	198.4988	198.5056	↗	3.9854
$\lambda_{6,h}$	236.8536	211.8241	208.0337	207.9773	207.9811	↗	2.9201

Table 3.3: Six minimum eigenvalues computed on Fig. 3.1(c) by the $\mathrm{sBDM}_3 - \mathrm{P}_2$ pair.

Mesh	0	1	2	3	4	Trend	Order
$\lambda_{1,h}$	22.0793	22.0815	22.0827	22.0829	22.0829	↗	3.5583
$\lambda_{2,h}$	34.2609	34.2679	34.2697	34.2701	34.2701	↗	3.4881
$\lambda_{3,h}$	42.5545	42.5414	42.5445	42.5451	42.5451	↗	3.4982
$\lambda_{4,h}$	53.8994	53.6110	53.6073	53.6082	53.6083	↗	3.2959
$\lambda_{5,h}$	58.4507	58.0302	58.0296	58.0310	58.0311	↗	3.3390
$\lambda_{6,h}$	72.9903	72.1440	72.1417	72.1438	72.1440	↗	3.3193

Table 3.4: Six minimum eigenvalues computed on Fig. 3.1(d) by the $\mathrm{sBDM}_3 - \mathrm{P}_2$ pair.

Mesh	0	1	2	3	4	Trend	Order
$\lambda_{1,h}$	31.9595	32.0371	32.0865	32.1108	32.1224	↗	1.0673
$\lambda_{2,h}$	37.1134	37.0358	37.0233	37.0198	37.0187	↘	1.7870
$\lambda_{3,h}$	41.9345	41.9283	41.9353	41.9378	41.9389	↗	1.1912
$\lambda_{4,h}$	49.0715	48.9836	48.9842	48.9838	48.9837	↘	1.1296
$\lambda_{5,h}$	55.4388	55.3719	55.3951	55.4059	55.4110	↗	1.1012
$\lambda_{6,h}$	69.5784	69.4105	69.4647	69.4895	69.5012	↗	1.0696

Table 3.5: Six minimum eigenvalues computed on Fig. 3.1(e) by the $\mathrm{sBDM}_3 - \mathrm{P}_2$ pair.

Mesh	0	1	2	3	4	Trend	Order
$\lambda_{1,h}$	24.3302	24.3507	24.3609	24.3650	24.3668	↗	1.2782
$\lambda_{2,h}$	42.2298	42.2277	42.2424	42.2485	42.2509	↗	1.3470
$\lambda_{3,h}$	42.5131	42.5000	42.5081	42.5122	42.5140	↗	1.1264
$\lambda_{4,h}$	59.2273	59.1436	59.1413	59.1421	59.1428	↗	0.3731
$\lambda_{5,h}$	63.8774	63.7937	63.8087	63.8156	63.8183	↗	1.3258
$\lambda_{6,h}$	76.4173	76.0611	76.0713	76.0761	76.0779	↗	1.4254

The numerical results show that as grids get refined,

(a) on the convex domains, the six minimum eigenvalues all show an increase trend;

(b) on the non-convex domains, we can observe that the six minimum eigenvalues are not always increasing, which is not deemed unacceptable as the theory in nonconvex domains are still challenging and rare.

3.2. A conservative finite element scheme of low-degree with $\mathcal{O}(h^2)$ accuracy on mildly-restricted grids

3.2.1. A smoothened Brezzi-Douglas-Fortin-Marini finite element space

An sBDFM_3 finite element is defined by the following triple $(T, \boldsymbol{P}_T, \boldsymbol{D}_T)$:

(1) T is a triangle;

(2) $P_T = \boldsymbol{P}_3^2(T) := \{\boldsymbol{v} \in \boldsymbol{P}_3(T) : \boldsymbol{v}\cdot\boldsymbol{n}_e \in P_2(e),\ \forall\, e \subset \partial T\}$;

(3) for any $\boldsymbol{v} \in (H^1(T))^2$, the nodal functionals on T, denoted by D_T, are

- $\fint_e (\boldsymbol{v}\cdot\boldsymbol{n})\tau^k \,\mathrm{d}\tau,\ k = 0,1,2,\ e \in \{e_1, e_2, e_3\}$;
- $\fint_e (\boldsymbol{v}\cdot\boldsymbol{t})\tau^k \,\mathrm{d}\tau,\ k = 0,1,\ e \in \{e_1, e_2, e_3\}$;
- $\fint_T \boldsymbol{v}^{(1)} \,\mathrm{d}x\mathrm{d}y,\ \fint_T \boldsymbol{v}^{(2)} \,\mathrm{d}x\mathrm{d}y$.

For the sBDFM$_3$ element, $\boldsymbol{D}_T$ is $\boldsymbol{P}_T$-unisolvent. Please refer to the first column of Table 5.1 for a specific choice of the degrees of freedom.

Define sBDFM$_3$ finite element spaces as follows:

$$\boldsymbol{V}_h^{\mathrm{sBDFM_3}} := \Big\{ \boldsymbol{v}_h \in \boldsymbol{H}(\mathrm{div},\Omega) : \boldsymbol{v}_h|_T \in \boldsymbol{P}_3^2(T),\ \forall\, T \in \mathcal{T}_h; \fint_e (\boldsymbol{v}_h\cdot\boldsymbol{t})\tau^k \mathrm{d}\tau (k=0,1) \text{ are continuous across interior edges } e \in \mathcal{E}_h^i \Big\}, \tag{3.9}$$

$$\boldsymbol{V}_{h0}^{\mathrm{sBDFM_3}} := \Big\{ \boldsymbol{v}_h \in \boldsymbol{V}_h^{\mathrm{sBDFM_3}} : \boldsymbol{v}_h\cdot\boldsymbol{n} = 0 \text{ and } \fint_e (\boldsymbol{v}_h\cdot\boldsymbol{t})\tau^k \mathrm{d}\tau = 0\ (k=0,1),\ \forall\, e \in \mathcal{E}_h^b \Big\}. \tag{3.10}$$

By definition, $\boldsymbol{V}_h^{\mathrm{sBDFM_3}} \subset \boldsymbol{H}(\mathrm{div},\Omega)$ but $\boldsymbol{V}_h^{\mathrm{sBDFM_3}} \not\subset \boldsymbol{H}^1(\Omega)$, and similarly $\boldsymbol{V}_{h0}^{\mathrm{sBDFM_3}} \subset H(\mathrm{div},\Omega)$ but $\boldsymbol{V}_{h0}^{\mathrm{sBDFM_3}} \not\subset \boldsymbol{H}^1(\Omega)$. Also, both $\boldsymbol{V}_h^{\mathrm{sBDFM_3}}$ and $\boldsymbol{V}_{h0}^{\mathrm{sBDFM_3}}$ are smoothened subspaces of the famous third-order BDFM finite element spaces with weak tangential continuity.

Define a nodal interpolation operator $\Pi_h : \boldsymbol{H}^1(\Omega) \to \boldsymbol{V}_h^{\mathrm{sBDFM_3}}$ such that for any $e \subset \mathcal{E}_h$,

$$\begin{aligned} \fint_e (\Pi_h\boldsymbol{v}\cdot\boldsymbol{n})\tau^k \mathrm{d}\tau &= \fint_e (\boldsymbol{v}\cdot\boldsymbol{n})\tau^k \mathrm{d}\tau, \quad k = 0,1,2, \\ \fint_e (\Pi_h\boldsymbol{v}\cdot\boldsymbol{t})\tau^k \mathrm{d}\tau &= \fint_e (\boldsymbol{v}\cdot\boldsymbol{t})\tau^k \mathrm{d}\tau, \quad k = 0,1. \end{aligned}$$

The operator is locally defined on each triangle, and is invariant under Piola's transformation. Moreover, Π_h preserves cubic polynomials locally. Therefore, approximation estimates of Π_h can be derived from [3, Lemma 2.1.5, Remark 2.1.8], along with standard scaling arguments and the Bramble-Hilbert lemma.

Proposition 3.2. *It holds for* $0 \le k \le 1 \le s \le 3$ *that*

$$|\boldsymbol{v} - \Pi_h\boldsymbol{v}|_{k,h} \lesssim h^{s-k}\,|\boldsymbol{v}|_{s,\Omega}, \quad \forall\, \boldsymbol{v} \in \boldsymbol{H}^s(\Omega). \tag{3.11}$$

3.2.2. Theoretical constructions of the scheme

Firstly, we introduce two types of macroelements and several definitions.

Definition 3.1. *A vertex-oriented macroelement M_A is defined as a union of elements which all have exactly one common vertex A in the interior of the macroelement, see Fig.* 3.3(a).

Definition 3.2. *An edge-oriented macroelement M_e is defined as four sequential elements sharing unique vertex with the interior edge e being the common edge of middle elements, see Fig.* 3.3(b).

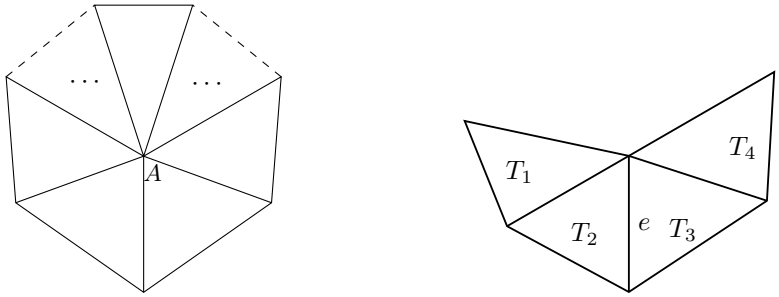

(a) M_A (b) M_e

Fig. 3.3. Two macroelements oriented by an interior vertex (left) and an interior edge (right).

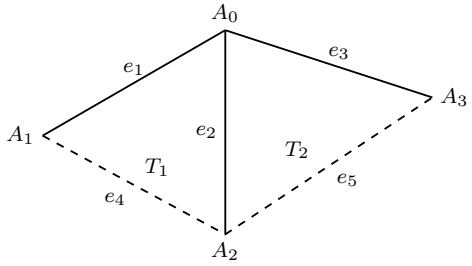

Fig. 3.4. Illustration of two adjacent cells within a macroelement.

Denote two signals on T_1 and T_2 in Fig. 3.4,

$$R_{12} := \frac{1}{l_2^2}\big(S_1\big(l_3^2 - l_5^2\big) + S_2\big(l_1^2 - l_4^2\big)\big),$$
$$Z_{12} := \frac{1}{2l_2^2}\big(S_1\big(11l_2^2 + 5l_5^2 - 5l_3^2\big) + S_2\big(11l_2^2 + 5l_4^2 - 5l_1^2\big)\big).$$

Denote $S_{12}^{in} := S_{\triangle(A_0,A_1,A_3)}$ and $S_{12}^{ex} := S_{\triangle(A_2,A_3,A_1)}$ respectively as areas of the cells with vertices $\{A_0, A_1, A_3\}$ and $\{A_2, A_3, A_1\}$, then it holds that

$$R_{12} = S_{12}^{in} - S_{12}^{ex}, \quad Z_{12} = 3S_{12}^{in} + 8S_{12}^{ex}, \quad 5R_{12} + 2Z_{12} = 11(S_1 + S_2).$$

Denote a signal on an edge-oriented macroelement M_e (cf. Fig. 3.3(b)) as follows:

$$F(e) := S_2 + S_3 + S_2\left(\frac{2R_{23}}{Z_{23}} + \frac{R_{34}}{Z_{34}}\right) + S_3\left(\frac{2R_{23}}{Z_{23}} + \frac{R_{12}}{Z_{12}}\right). \tag{3.12}$$

Assumption 3.1. For any m-cell vertex-oriented macroelement, if m is an even number and $Z_{12}Z_{23}\cdots Z_{m1} \neq 0$, then there are not three sequential interior edges simultaneously satisfying $F(e) = 0$, where $F(e)$ is referred to (3.12).

Now consider the finite element discretization: Find $(\boldsymbol{u}_h, p_h) \in \boldsymbol{V}_{h0}^{\mathrm{sBDFM}_3} \times Q_{h*}^2$ such that

$$\begin{cases} \varepsilon^2(\nabla_h \boldsymbol{u}_h, \nabla_h \boldsymbol{v}_h) - (\operatorname{div} \boldsymbol{v}_h, p_h) = (\boldsymbol{f}, \boldsymbol{v}_h), & \forall\, \boldsymbol{v}_h \in \boldsymbol{V}_{h0}^{\mathrm{sBDFM}_3}, \\ (\operatorname{div} \boldsymbol{u}_h, q_h) = 0, & \forall\, q_h \in Q_{h*}^2. \end{cases} \tag{3.13}$$

The space for pressure follows from (3.4). This finite element scheme is denoted by $\mathrm{sBDFM}_3 - \mathrm{P}_2$.

Lemma 3.3 (Stability of $\boldsymbol{V}_{h0}^{\mathrm{sBDFM}_3} \times Q_{h*}^2$). *Let $\mathcal{T}_h$ be a family of triangulations of Ω satisfying Assumptions* 2.1*,* 2.2*,* 3.1*. Then it holds that*

$$\inf_{q_h \in Q_{h*}^2} \sup_{\boldsymbol{v}_h \in \boldsymbol{V}_{h0}^{\mathrm{sBDFM}_3}} \frac{(\mathrm{div}\boldsymbol{v}_h, q_h)}{\|q_h\|_{0,\Omega}\|\boldsymbol{v}_h\|_{1,h}} \geqslant C > 0. \tag{3.14}$$

We postpone the proof of Lemma 3.3 to Section 5. The discrete Korn inequality holds for $\boldsymbol{V}_{h0}^{\mathrm{sBDFM}_3} \subset \boldsymbol{V}_{h0}^{\mathrm{sBDM}_3}$ that

$$\|\boldsymbol{u}\|_{1,h}^2 \leqslant C \sum_{T \in \mathcal{T}_h} \|\epsilon(\boldsymbol{u})\|_{0,T}^2, \quad \forall\, \boldsymbol{u} \in \boldsymbol{V}_{h0}^{\mathrm{sBDFM}_3}. \tag{3.15}$$

It follows that (3.13) is a stable and conservative discretization scheme and its well-posedness is immediate.

Remark 3.1. We remark that, Assumption 3.1 is proposed to exclude a very special class of grids, and most grids satisfy the assumption. For example, the widely accepted well-centered triangulation given by [23] satisfy it. For this kind of triangulations, each simplex contains its circumcenter in its interior, and it ensures that $S_{i,i+1}^{in} > 0, S_{i,i+1}^{ex} > 0, Z_{i,i+1} \neq 0$ and thus $F(e) \neq 0$, $\forall e \in \mathcal{E}_h^i$.

Theorem 3.2. *Let $(\boldsymbol{u}, p)$ and $(\boldsymbol{u}_h, p_h)$ be the solutions of* (2.2) *and* (3.13)*, respectively. If $(\boldsymbol{u}, p) \in \boldsymbol{H}^3(\Omega) \times H^2(\Omega)$, then*

$$|\boldsymbol{u} - \boldsymbol{u}_h|_{1,h} \leqslant Ch^2|\boldsymbol{u}|_{3,\Omega}, \quad \|p - p_h\|_{0,\Omega} \leqslant Ch^2|p|_{2,\Omega} + C\varepsilon^2 h^2|\boldsymbol{u}|_{3,\Omega}.$$

3.2.3. Numerical experiments

This subsubsection is arranged analogously to Section 3.1.3: Example 3.3 is carried out to test the convergence rate of the $\mathrm{sBDFM}_3 - \mathrm{P}_2$ scheme and Example 3.4 aims at exploring the numerical performance when utilized to solve the Stokes eigenvalue problem (3.8). It deserves to be mentioned that the $\mathrm{sBDFM}_3 - \mathrm{P}_2$ pair is observed to provide upper bounds for the exact eigenvalues of (3.8).

Example 3.3. This example considers the Stokes problem (2.1) and it has the same domains and exact solutions as in Example 3.1. The following figures about the convergence rate are obtained by the discretization scheme: $\mathrm{sBDFM}_3 - \mathrm{P}_2$.

Fig. 3.5 indicates that consistent with Theorem 3.2, the velocity errors in $\boldsymbol{H}^1$-norm are of $\mathcal{O}(h^2)$ order and $\boldsymbol{L}^2$-norm are of $\mathcal{O}(h^3)$ order; the pressure errors in L^2-norm are of $\mathcal{O}(h^2)$ order.

Example 3.4. Consider the discrete form of (3.8): find $(\boldsymbol{u}_h, p_h) \in \boldsymbol{V}_{h0}^{\mathrm{sBDFM}_3} \times Q_{h*}^2$ and $\lambda \in \mathbb{R}$ such that

$$\begin{cases} \big(\nabla_h\, \boldsymbol{u}_h, \nabla\, \boldsymbol{v}_h\big) - (\mathrm{div}\, \boldsymbol{v}_h, p_h) = \lambda(\boldsymbol{u}_h, \boldsymbol{v}_h), & \forall\, \boldsymbol{v}_h \in \boldsymbol{V}_{h0}^{\mathrm{sBDFM}_3}, \\ (\mathrm{div}\, \boldsymbol{u}_h, q_h) = 0, & \forall\, q_h \in Q_{h*}^2. \end{cases}$$

The simulations are performed on the five domains in Fig. 3.1 and six minimum eigenvalues are recorded in Tables 3.6-3.10.

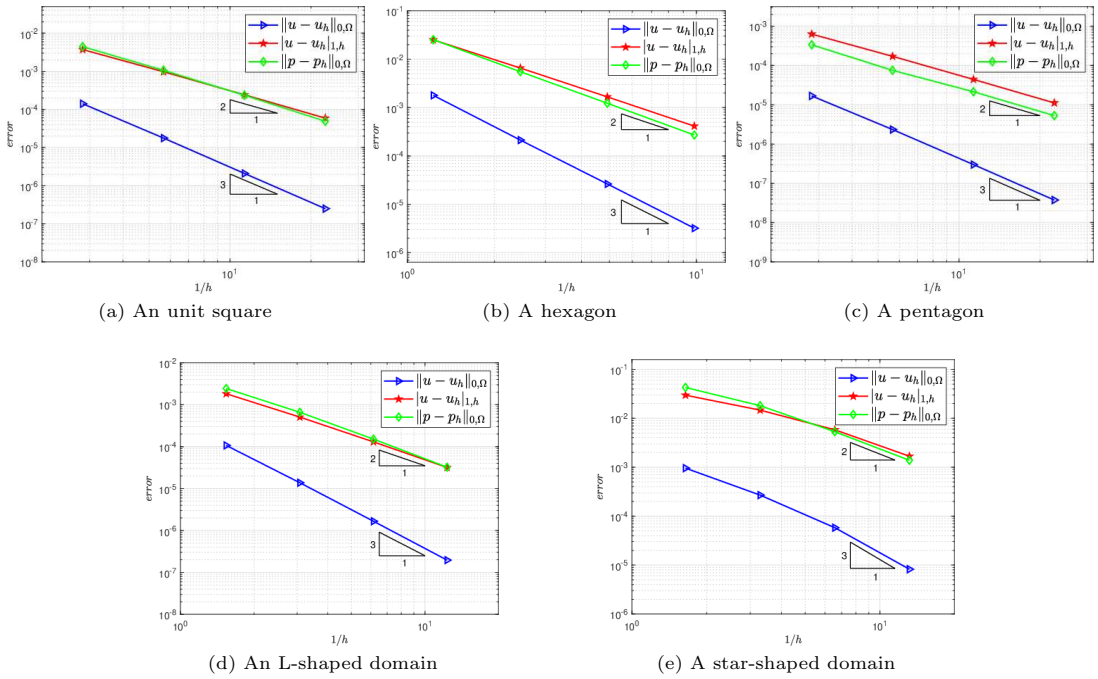

(a) An unit square (b) A hexagon (c) A pentagon

(d) An L-shaped domain (e) A star-shaped domain

Fig. 3.5. Velocity errors in the L^2- and H^1-norm and pressure errors in the L^2-norm by the sBDFM$_3$ − P$_2$ pair on five domains.

Table 3.6: Six minimum eigenvalues computed on Fig. 3.1(a) by the sBDFM$_3$ − P$_2$ pair.

Mesh	0	1	2	3	4	Trend	Order
$\lambda_{1,h}$	53.2285	52.4209	52.3496	52.3450	52.3447	↘	4.1015
$\lambda_{2,h}$	95.0649	92.3658	92.1405	92.1254	92.1245	↘	4.0596
$\lambda_{3,h}$	96.7211	92.4833	92.1479	92.1258	92.1245	↘	4.0545
$\lambda_{4,h}$	140.3577	129.2185	128.2780	128.2137	128.2098	↘	4.0535
$\lambda_{5,h}$	162.9623	155.0965	154.1894	154.1294	154.1257	↘	4.0272
$\lambda_{6,h}$	177.6041	168.2320	167.1128	167.0344	167.0295	↘	4.0070

Table 3.7: Six minimum eigenvalues computed on Fig. 3.1(b) by the sBDFM$_3$ − P$_2$ pair.

Mesh	0	1	2	3	4	Trend	Order
$\lambda_{1,h}$	81.4108	80.8408	80.7545	80.7468	80.7462	↘	3.7594
$\lambda_{2,h}$	107.8438	103.5686	103.1621	103.1274	103.1248	↘	3.7824
$\lambda_{3,h}$	164.6074	150.8761	149.5314	149.4331	149.4268	↘	3.9475
$\lambda_{4,h}$	172.6789	170.0333	169.7503	169.7255	169.7235	↘	3.6811
$\lambda_{5,h}$	203.0663	199.6669	198.6094	198.5138	198.5062	↘	3.6620
$\lambda_{6,h}$	257.7784	211.6450	208.2410	207.9974	207.9821	↘	3.9947

Table 3.8: Six minimum eigenvalues computed on Fig. 3.1(c) by the $\mathrm{sBDFM}_3 - \mathrm{P}_2$ pair.

Mesh	0	1	2	3	4	Trend	Order
$\lambda_{1,h}$	22.4482	22.1180	22.0852	22.0830	22.0829	$\searrow$	4.0363
$\lambda_{2,h}$	36.2739	34.4362	34.2813	34.2708	34.2701	$\searrow$	4.0202
$\lambda_{3,h}$	44.3672	42.7085	42.5558	42.5458	42.5451	$\searrow$	4.0214
$\lambda_{4,h}$	59.6039	54.1136	53.6465	53.6107	53.6084	$\searrow$	3.9983
$\lambda_{5,h}$	63.0435	58.5698	58.0698	58.0336	58.0313	$\searrow$	3.9869
$\lambda_{6,h}$	78.2625	72.9801	72.2092	72.1482	72.1443	$\searrow$	3.9747

Table 3.9: Six minimum eigenvalues computed on Fig. 3.1(d) by the $\mathrm{sBDFM}_3 - \mathrm{P}_2$ pair.

Mesh	0	1	2	3	4	Trend	Order
$\lambda_{1,h}$	32.8905	32.2642	32.1680	32.1462	32.1386	$\searrow$	1.5199
$\lambda_{2,h}$	37.6174	37.0927	37.0291	37.0206	37.0189	$\searrow$	2.3139
$\lambda_{3,h}$	43.1411	42.0289	41.9457	41.9405	41.9402	$\searrow$	3.8531
$\lambda_{4,h}$	51.6194	49.1801	48.9984	48.9848	48.9837	$\searrow$	3.6762
$\lambda_{5,h}$	59.1626	55.7099	55.4445	55.4214	55.4178	$\searrow$	2.6603
$\lambda_{6,h}$	73.8393	70.0391	69.5869	69.5302	69.5186	$\searrow$	2.2908

Table 3.10: Six minimum eigenvalues computed on Fig. 3.1(e) by the $\mathrm{sBDFM}_3 - \mathrm{P}_2$ pair.

Mesh	0	1	2	3	4	Trend	Order
$\lambda_{1,h}$	24.7992	24.4429	24.3865	24.3740	24.3702	$\searrow$	1.7061
$\lambda_{2,h}$	43.2838	42.3508	42.2648	42.2550	42.2532	$\searrow$	2.4232
$\lambda_{3,h}$	44.1901	42.7303	42.5637	42.5312	42.5214	$\searrow$	1.7256
$\lambda_{4,h}$	60.9213	59.3323	59.1661	59.1478	59.1447	$\searrow$	2.5424
$\lambda_{5,h}$	65.9695	64.0544	63.8469	63.8258	63.8220	$\searrow$	2.4893
$\lambda_{6,h}$	79.3820	76.5305	76.1470	76.0982	76.0861	$\searrow$	2.0122

The numerical results show that:

(a) The six minimum eigenvalues are decreasing strictly with mesh refinements not only in convex domains but also in nonconvex domains.

(b) The convergence order in convex domains approximates $\mathcal{O}(h^4)$, square of the convergence rate of the eigenfunctions, which represents excellent agreement with the theoretical prediction of [28], robustly validating our numerical scheme.

4. Proof of Lemma 3.1

In this section, we validate the four conditions of Stenberg's macroelement technique (see Proposition 2.1) for the $\mathrm{sBDM}_3 - \mathrm{P}_2$ scheme. To unfold it, Lemmas 4.1 and 4.2 show that the condition C_1 holds on an edge-oriented macroelement and a three-cell vertex-oriented macroele-

ment respectively, and the latter is just a special case of the former; Lemma 4.3 demonstrates that the conditions C_2, C_3 and C_4 hold. We firstly write the details on a local cell as a separate subsection (Section 4.1) as preparation for the subsequent discussions in Section 4.2.

4.1. Structure of the kernel space of the divergence operator on a cell

The local directions of $\boldsymbol{t}_j, \boldsymbol{n}_j, \boldsymbol{t}_k, \boldsymbol{n}_k$ are shown in Fig. 4.1 and thus every local cell can be embedded into Fig. 4.2(a) straightforwardly. Table 4.1 exhibits a set of locally defined functions $\boldsymbol{\psi}_{s,T}, s = 1:8$ and $\mathrm{span}\{\boldsymbol{\psi}_{s,T}\}_{s=1:8}$ forms a basis of the kernel space of the divergence operator on a local cell T with nodal parameters vanished on edge e_i. It reveals that $\fint_{e_j} \boldsymbol{\psi}_{s,T} \cdot \boldsymbol{n}_j \,\mathrm{d}\tau = \fint_{e_k} \boldsymbol{\psi}_{s,T} \cdot \boldsymbol{n}_k \,\mathrm{d}\tau = 0, s = 1:7$ and $\fint_{e_j} \boldsymbol{\psi}_{8,T} \cdot \boldsymbol{n}_j \,\mathrm{d}\tau \neq 0, \fint_{e_k} \boldsymbol{\psi}_{8,T} \cdot \boldsymbol{n}_k \,\mathrm{d}\tau \neq 0$. Furthermore, $\{\boldsymbol{\psi}_{1,T}, \boldsymbol{\psi}_{3,T}\}$ are nonzero only on the edge e_j and $\{\boldsymbol{\psi}_{2,T}, \boldsymbol{\psi}_{4,T}\}$ are nonzero only on the edge e_k in the sense of nodal parameters.

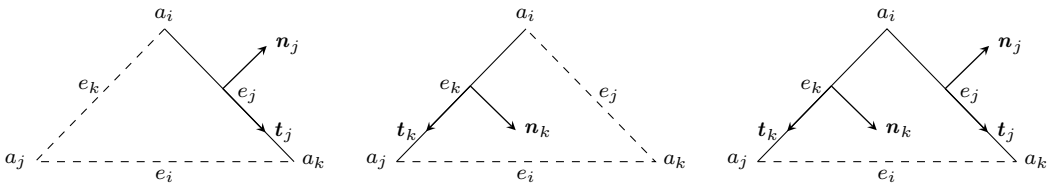

Fig. 4.1. Illustration of the supports of locally defined basis functions; nodal parameters vanish on dotted edges.

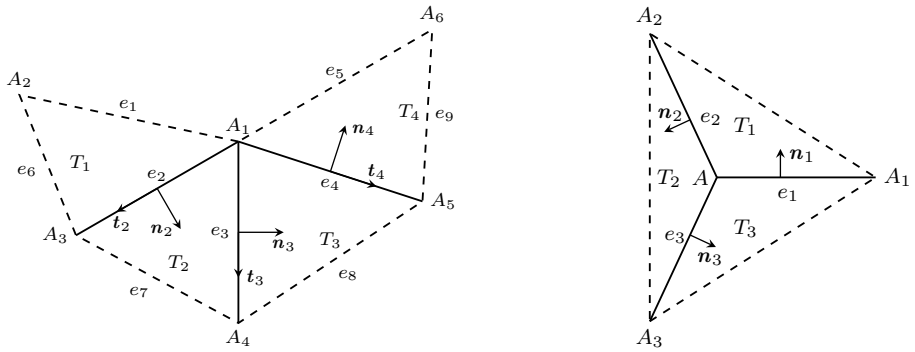

(a) M_{e_3} (b) M_A

Fig. 4.2. An interior edge oriented macroelement (left) and its degeneration circumstance (right).

4.2. Verification of the four conditions of Stenberg's technique (Proposition 2.1)

Given a macroelement M_e, we define

$$\boldsymbol{V}_{h0,M_e}^{\mathrm{sBDM}_3} := \Big\{ \boldsymbol{v}_h \in \boldsymbol{H}(\mathrm{div}, M_e) : \boldsymbol{v}_h|_T \in \boldsymbol{P}_3(T),\ \forall\, T \in M_e;\ \boldsymbol{v}_h \cdot \boldsymbol{n} \text{ and } \fint_e (\boldsymbol{v}_h \cdot \boldsymbol{t})\tau^k \mathrm{d}\tau\ (k = 0, 1)$$
$$\text{are continuous across interior edges and vanish on the edges lying on } \partial M_e \Big\},$$

Table 4.1: Locally defined div-free functions with nodal parameters vanished on the edge e_i.

$\boldsymbol{\psi}$	$\boldsymbol{\psi}_{1,T}$	$\boldsymbol{\psi}_{2,T}$	$\boldsymbol{\psi}_{3,T}$	$\boldsymbol{\psi}_{4,T}$	$\boldsymbol{\psi}_{5,T}$	$\boldsymbol{\psi}_{6,T}$	$\boldsymbol{\psi}_{7,T}$	$\boldsymbol{\psi}_{8,T}$
$\fint_{e_j} \boldsymbol{\psi}\cdot\boldsymbol{n}_j \mathrm{d}\tau$	0	0	0	0	0	0	0	$-2Sl_jl_k^2$
$\fint_{e_j} \boldsymbol{\psi}\cdot\boldsymbol{n}_j(\lambda_k-\lambda_i)\mathrm{d}\tau$	0	0	$-\frac{2S}{l_j}$	0	0	0	0	$2Sl_jl_k^2$
$30\fint_{e_j} \boldsymbol{\psi}\cdot\boldsymbol{n}_j\left(\frac{1}{6}-\lambda_k\lambda_i\right)\mathrm{d}\tau$	0	0	0	0	$\frac{2S}{l_j}$	0	0	$4Sl_j\left(l_i^2-l_j^2+2l_k^2\right)$
$7\fint_{e_j} \boldsymbol{\psi}\cdot\boldsymbol{n}_j\Big(\frac{5}{2}(\lambda_k-\lambda_i)^3 -\frac{3}{2}(\lambda_k-\lambda_i)\Big)\mathrm{d}\tau$	$\frac{2S}{l_j}$	0	$\frac{11S}{l_j}$	0	$\frac{S}{l_j}$	0	0	$-\frac{S}{l_j}\big(3l_i^2l_j^2-l_i^2l_k^2 -3l_j^4+4l_j^2l_k^2+l_k^4\big)$
$\fint_{e_j} \boldsymbol{\psi}\cdot\boldsymbol{t}_j \mathrm{d}\tau$	l_j	0	0	0	0	l_j	$-5l_j$	0
$\fint_{e_j} \boldsymbol{\psi}\cdot\boldsymbol{t}_j(\lambda_k-\lambda_i)\mathrm{d}\tau$	0	0	$\frac{l_k^2-l_i^2}{2l_j}$	0	$\frac{l_j}{2}$	0	l_j	$\frac{l_j}{2}\big(l_i^2l_j^2+l_i^2l_k^2 -l_j^4+4l_j^2l_k^2-l_k^4\big)$
$\fint_{e_k} \boldsymbol{\psi}\cdot\boldsymbol{n}_k \mathrm{d}\tau$	0	0	0	0	0	0	0	$-2Sl_j^2l_k$
$\fint_{e_k} \boldsymbol{\psi}\cdot\boldsymbol{n}_k(\lambda_j-\lambda_i)\mathrm{d}\tau$	0	0	0	$\frac{2S}{l_k}$	0	0	0	$2Sl_j^2l_k$
$30\fint_{e_k} \boldsymbol{\psi}\cdot\boldsymbol{n}_k\left(\frac{1}{6}-\lambda_j\lambda_i\right)\mathrm{d}\tau$	0	0	0	0	0	$-\frac{2S}{l_k}$	0	0
$7\fint_{e_k} \boldsymbol{\psi}\cdot\boldsymbol{n}_k\Big(\frac{5}{2}(\lambda_j-\lambda_i)^3 -\frac{3}{2}(\lambda_j-\lambda_i)\Big)\mathrm{d}\tau$	0	$-\frac{2S}{l_k}$	0	$-\frac{11S}{l_k}$	0	$-\frac{S}{l_k}$	0	0
$\fint_{e_k} \boldsymbol{\psi}\cdot\boldsymbol{t}_k \mathrm{d}\tau$	0	l_k	0	0	l_k	0	$5l_k$	0
$\fint_{e_k} \boldsymbol{\psi}\cdot\boldsymbol{t}_k(\lambda_j-\lambda_i)\mathrm{d}\tau$	0	0	0	$\frac{l_j^2-l_i^2}{2l_k}$	0	$\frac{l_k}{2}$	$-l_k$	0
$\fint_T \boldsymbol{\psi}^{(1)}\mathrm{d}x\mathrm{d}y$	0	0	x_i-x_k	x_i-x_j	0	0	0	0
$\fint_T \boldsymbol{\psi}^{(2)}\mathrm{d}x\mathrm{d}y$	0	0	y_i-y_k	y_i-y_j	0	0	0	0

$$\boldsymbol{V}_{h0,M_A}^{\mathrm{sBDM}_3} := \Big\{ \boldsymbol{v}_h \in \boldsymbol{H}(\mathrm{div}, M_A) : \boldsymbol{v}_h|_T \in \boldsymbol{P}_3(T),\ \forall T \in M_A;\ \boldsymbol{v}_h\cdot\boldsymbol{n} \text{ and } \fint_e (\boldsymbol{v}_h\cdot\boldsymbol{t})\tau^k \mathrm{d}\tau\ (k=0,1) \text{ are continuous across interior edges and vanish on the edges lying on } \partial M_A \Big\}.$$

Lemma 4.1. *For an edge-oriented macroelement M_{e_3} (see Fig. 4.2), the space*

$$N_{M_{e_3}} := \Big\{ q_h \in Q_{h,M_{e_3}}^2 : \int_{M_{e_3}} \mathrm{div}\, \boldsymbol{v}_h\, q_h = 0,\ \forall\, \boldsymbol{v}_h \in \boldsymbol{V}_{h0,M_{e_3}}^{\mathrm{sBDM}_3} \Big\}$$

is a one-dimensional space consisting of constant functions on M_{e_3}.

Proof. By definition, it holds $\mathrm{div}(\boldsymbol{V}_{h0,M_{e_3}}^{\mathrm{sBDM}_3}) \subset Q_{h*,M_{e_3}}^2$. If $\dim(\ker(\mathrm{div}, \boldsymbol{V}_{h0,M_{e_3}}^{\mathrm{sBDM}_3})) = 3$, then by

$$\dim\Big(\mathrm{div}\Big(\boldsymbol{V}_{h0,M_{e_3}}^{\mathrm{sBDM}_3}\Big)\Big) + \dim\Big(\ker\Big(\mathrm{div}, \boldsymbol{V}_{h0,M_{e_3}}^{\mathrm{sBDM}_3}\Big)\Big) = \dim\Big(\boldsymbol{V}_{h0,M_{e_3}}^{\mathrm{sBDM}_3}\Big),$$

we can derive

$$\dim\left(\operatorname{div}\left(\boldsymbol{V}_{h0,M_{e_3}}^{\mathrm{sBDM}_3}\right)\right)=23=\dim\left(Q_{h*,M_{e_3}}^2\right)$$

and further $\operatorname{div}(\boldsymbol{V}_{h0,M_{e_3}}^{\mathrm{sBDM}_3})=Q_{h*,M_{e_3}}^2$, which trivially concludes that $\dim N_{M_{e_3}}=1$ and $N_{M_{e_3}}$ consists of sonstant functions on M_{e_3}.

Therefore, the entire proof is reduced to show

$$\dim\left(\ker\left(\operatorname{div},\,\boldsymbol{V}_{h0,M_{e_3}}^{\mathrm{sBDM}_3}\right)\right)=3.$$

Assume $\boldsymbol{v}_h\in\ker(\operatorname{div},\,\boldsymbol{V}_{h0,M_{e_3}}^{\mathrm{sBDM}_3})$, with

$$\boldsymbol{v}_h|_T=\sum_{s=1:8}c_{s,T}\boldsymbol{\psi}_{s,T},\quad\forall\,T\in M_{e_3}.$$

Firstly, on T_1 and T_4 it holds that

$$\boldsymbol{v}_h|_{T_1}\in\operatorname{span}\{\boldsymbol{\psi}_{1,T_1},\,\boldsymbol{\psi}_{3,T_1}\},\quad \boldsymbol{v}_h|_{T_4}\in\operatorname{span}\{\boldsymbol{\psi}_{2,T_4},\,\boldsymbol{\psi}_{4,T_4}\}.$$

Further, by Table 4.1 we obtain

$$\begin{aligned}\boldsymbol{v}_h|_{T_2}&\in\operatorname{span}\{\boldsymbol{\psi}_{1,T_2},\,\boldsymbol{\psi}_{2,T_2},\,\boldsymbol{\psi}_{3,T_2},\,\boldsymbol{\psi}_{4,T_2},\,\boldsymbol{\psi}_{5,T_2},\,\boldsymbol{\psi}_{7,T_2}\},\\ \boldsymbol{v}_h|_{T_3}&\in\operatorname{span}\{\boldsymbol{\psi}_{1,T_3},\,\boldsymbol{\psi}_{2,T_3},\,\boldsymbol{\psi}_{3,T_3},\,\boldsymbol{\psi}_{4,T_3},\,\boldsymbol{\psi}_{6,T_3},\,\boldsymbol{\psi}_{7,T_3}\}.\end{aligned}$$

Specifically, considering the continuities on e_2, we reach such relations

$$\begin{aligned}c_{2,T_2}&=-\frac{S_1}{S_2}c_{1,T_1},&&&c_{4,T_2}&=-\frac{S_1}{S_2}c_{3,T_1},\\ c_{5,T_2}&=\frac{S_1+S_2}{S_2}c_{1,T_1}+\frac{5R_{12}}{2S_2}c_{3,T_1},&&&c_{7,T_2}&=-\frac{R_{12}}{2S_2}c_{3,T_1},\end{aligned}\tag{4.1}$$

which suggests that $\{c_{1,T_1},\,c_{3,T_1},\,c_{2,T_2},\,c_{4,T_2}\}$ can be consequently obtained once $\{c_{5,T_2},\,c_{7,T_2}\}$ are computed.

Likewise, the continuities on e_4 lead to

$$\begin{aligned}c_{1,T_3}&=-\frac{S_4}{S_3}c_{2,T_4},&&&c_{3,T_3}&=-\frac{S_4}{S_3}c_{4,T_4},\\ c_{6,T_3}&=\frac{S_3+S_4}{S_3}c_{2,T_4}+\frac{5R_{34}}{2S_3}c_{4,T_4},&&&c_{7,T_3}&=\frac{R_{34}}{2S_3}c_{4,T_4},\end{aligned}\tag{4.2}$$

which implies that $\{c_{2,T_4},\,c_{4,T_4},\,c_{6,T_3},\,c_{7,T_3}\}$ can be immediately obtained once $\{c_{6,T_3},\,c_{7,T_3}\}$ are computed.

Now we consider the continuites on e_3

$$\begin{bmatrix}\boldsymbol{\psi}_{1,T_2} & \boldsymbol{\psi}_{3,T_2} & \boldsymbol{\psi}_{5,T_2} & \boldsymbol{\psi}_{7,T_2}\end{bmatrix}\Big|_{e_3}\begin{bmatrix}c_{1,T_2}\\ c_{3,T_2}\\ c_{5,T_2}\\ c_{7,T_2}\end{bmatrix}=\begin{bmatrix}\boldsymbol{\psi}_{2,T_3} & \boldsymbol{\psi}_{4,T_3} & \boldsymbol{\psi}_{6,T_3} & \boldsymbol{\psi}_{7,T_3}\end{bmatrix}\Big|_{e_3}\begin{bmatrix}c_{2,T_3}\\ c_{4,T_3}\\ c_{6,T_3}\\ c_{7,T_3}\end{bmatrix}.$$

With the help of Table 4.1, we can establish the following system:

$$\begin{bmatrix} 0 & -\frac{2S_2}{l_3} & 0 & 0 & 0 & -\frac{2S_3}{l_3} & 0 & 0 \\ 0 & 0 & \frac{2S_2}{l_3} & 0 & 0 & 0 & \frac{2S_3}{l_3} & 0 \\ \frac{2S_2}{l_3} & \frac{11S_2}{l_3} & \frac{11S_3}{l_3} & \frac{S_2}{l_3} & 0 & \frac{2S_3}{l_3} & \frac{S_3}{l_3} & 0 \\ l_3 & 0 & 0 & -5l_3 & -l_3 & 0 & 0 & -5l_3 \\ 0 & \frac{l_2^2-l_7^2}{2l_3} & \frac{l_3}{2} & l_3 & 0 & -\frac{l_4^2-l_8^2}{2l_3} & -\frac{l_3}{2} & l_3 \end{bmatrix} \begin{bmatrix} c_{1,T_2} \\ c_{3,T_2} \\ c_{5,T_2} \\ c_{7,T_2} \\ c_{2,T_3} \\ c_{4,T_3} \\ c_{6,T_3} \\ c_{7,T_3} \end{bmatrix} = \begin{bmatrix} 0 \\ 0 \\ 0 \\ 0 \\ 0 \end{bmatrix}.$$

The rank of the coefficient matrix is 5, thus the solution space is 3-dimension, which together with the analysis of (4.1) and (4.2) shows $\dim(\ker(\mathrm{div}, \boldsymbol{V}_{h0,M_{e_3}}^{\mathrm{sBDM}_3})) = 3$. □

In particular, if the exterior cells T_1 and T_4 in Fig. 4.2(a) are superimposed, the edge-oriented macroelement M_{e_3} degenerates into a closed patch as depicted in Fig. 4.2(b), which is exactly a 3-cell vertex-oriented macroelement M_A.

Lemma 4.2. *For a three-cell vertex-oriented macroelement M_A, the space*

$$N_{M_A} := \left\{ q_h \in Q_{h,M_A} : \int_{M_A} \mathrm{div}\boldsymbol{v}_h \; q_h = 0, \; \forall\, \boldsymbol{v}_h \in \boldsymbol{V}_{h0,M_A}^{\mathrm{sBDM}_3} \right\}$$

is one-dimensional space consisting of constant functions on M_A.

The proof idea of Lemma 4.2 is similar to that of Lemma 4.1 and we refer to Appendix A.1 for a thorough proof.

Lemma 4.3. *Let $\mathcal{T}_h$ be a family of triangulations of Ω satisfying Assumptions* 2.1 *and* 2.2. *The macroelement triangulation $\mathcal{M}_h$ consists of all edge-oriented macroelements and all three-cell vertex-oriented macroelements. Then the conditions C_2, C_3 and C_4 presented in Proposition* 2.1 *holds.*

Proof. By Assumption 2.2, $\mathcal{M}_h$ defined above includes two classes of equivalent macroelements, then condition C_2 holds. For any $e \in \mathcal{E}_h^i$, it exists in at least one edge-oriented macroelement or one three-cell vertex-oriented macroelement and at most five edge-oriented macroelements where the five edges (including itself) are exactly edges sharing vertexes with e. Therefore condition C_3 is satisfied. Moreover, condition C_4 is obtained by Proposition 3.1 and the well-known trace theorem(see, e.g., [4, Theorem 1.6.6]). □

5. Proof of Lemma 3.3

The section aims at proving the inf-sup stability of the finite element spaces pair $\boldsymbol{V}_{h0}^{\mathrm{sBDFM}_3} \times Q_{h*}^2$ (Lemma 3.3) by Stenberg's macroelement technique (Proposition 2.1). As a centerpiece of this current section, Section 5.2 presents the verification of the four conditions in Proposition 2.1. Specifically, Lemmas 5.3 and 5.4 show that the condition C_1 holds on a vertex-oriented macroelement and an edge-oriented macroelement respectively; Lemma 5.5 shows that the conditions C_2, C_3 and C_4 hold for a certain definition of macroelement triangulations $\mathcal{M}_h$. In addition, Section 5.1 gives a thorough interpretation of the kernel of the divergence operator on a local cell, serving Section 5.2.

5.1. Structure of the kernel space of the divergence operator on a cell

The local directions of $\boldsymbol{t}_j, \boldsymbol{n}_j, \boldsymbol{t}_k, \boldsymbol{n}_k$ are shown in Fig. 4.1 and thus every local cell can be embedded into Fig. 5.3(b) straightforwardly. Table 5.1 exhibits a set of locally defined functions $\boldsymbol{\omega}_{s,T}, s = 1:6$ and $\mathrm{span}\{\boldsymbol{\omega}_{s,T}\}_{s=1:6}$ forms a basis of the kernel space of the divergence operator on a local cell T with nodal parameters vanished on edge e_i. It reveals that $\fint_{e_j} \boldsymbol{\omega}_{s,T} \cdot \boldsymbol{n}_j \,\mathrm{d}\tau = \fint_{e_k} \boldsymbol{\omega}_{s,T} \cdot \boldsymbol{n}_k \,\mathrm{d}\tau = 0, s = 1:5$ and $\fint_{e_j} \boldsymbol{\omega}_{6,T} \cdot \boldsymbol{n}_j \,\mathrm{d}\tau \neq 0, \fint_{e_k} \boldsymbol{\omega}_{6,T} \cdot \boldsymbol{n}_k \,\mathrm{d}\tau \neq 0$. Furthermore, $\boldsymbol{\omega}_{1,T}$ is nonzero only on e_j and $\boldsymbol{\omega}_{2,T}$ is nonzero only on e_k in the sense of nodal parameters.

Remark 5.1. Refer to Fig. 5.1 and investigate the geometric significance of $Z_{12} = 0$ for adjacent units $T_1 \cup T_2$. Since by definition $Z_{12} = 3S_{12}^{in} + 8S_{12}^{ex} = 0$ and $S_{12}^{in} + S_{12}^{ex} = S_1 + S_2 > 0$, it can be obtained that $S_{12}^{in} > 0, S_{12}^{ex} < 0$ and $S_{12}^{ex}/S_{12}^{in} = -3/5$. Prolong A_1A_3 to A_4 until $|A_1A_3|/|A_3A_4| = 5/3$, then $T_1 = \triangle(A_1, A_2, A_3)$ and $T_2 = \triangle(A_1, A_3, B)$ satisfy $Z_{12} = 0$ if and only if B lands on the extension cord of A_2A_4 (e.g., $B = B_i, i = 1:4$), and in this case it must be true that $|A_1A_3| < |A_1B|$.

Based on Remark 5.1, the following lemma can be proved by contradiction and it plays a crucial role in the proof of Lemma 5.2.

Table 5.1: Locally defined div-free functions with nodal parameters vanished on the edge e_i.

$\boldsymbol{\omega}$	$\boldsymbol{\omega}_{1,T}$	$\boldsymbol{\omega}_{2,T}$	$\boldsymbol{\omega}_{3,T}$	$\boldsymbol{\omega}_{4,T}$	$\boldsymbol{\omega}_{5,T}$	$\boldsymbol{\omega}_{6,T}$
$\fint_{e_j} \boldsymbol{\omega} \cdot \boldsymbol{n}_j \,\mathrm{d}\tau$	0	0	0	0	0	$-2Sl_jl_k^2$
$\fint_{e_j} \boldsymbol{\omega} \cdot \boldsymbol{n}_j \,(\lambda_k - \lambda_i) \,\mathrm{d}\tau$	$-\frac{2S}{l_j}$	0	0	0	0	$2Sl_jl_k^2$
$30\fint_{e_j} \boldsymbol{\omega} \cdot \boldsymbol{n}_j \left(\frac{1}{6} - \lambda_k\lambda_i\right) \mathrm{d}\tau$	0	0	$\frac{2S}{l_j}$	0	0	$4Sl_j(l_i^2 - l_j^2 + 2l_k^2)$
$\fint_{e_j} \boldsymbol{\omega} \cdot \boldsymbol{t}_j \,\mathrm{d}\tau$	0	0	0	l_j	$-5l_j$	$\frac{l_j}{2}(3l_i^2l_j^2 - l_i^2l_k^2 - 3l_j^4 + 4l_j^2l_k^2 + l_k^4)$
$\fint_{e_j} \boldsymbol{\omega} \cdot \boldsymbol{t}_j \,(\lambda_k - \lambda_i) \,\mathrm{d}\tau$	$\frac{l_k^2 - l_i^2}{2l_j}$	0	$\frac{l_j}{2}$	0	l_j	$\frac{l_j}{2}(l_i^2l_j^2 + l_i^2l_k^2 - l_j^4 + 4l_j^2l_k^2 - l_k^4)$
$\fint_{e_k} \boldsymbol{\omega} \cdot \boldsymbol{n}_k \,\mathrm{d}\tau$	0	0	0	0	0	$-2Sl_j^2l_k$
$\fint_{e_k} \boldsymbol{\omega} \cdot \boldsymbol{n}_k \,(\lambda_j - \lambda_i) \,\mathrm{d}\tau$	0	$\frac{2S}{l_k}$	0	0	0	$2Sl_j^2l_k$
$30\fint_{e_k} \boldsymbol{\omega} \cdot \boldsymbol{n}_k \left(\frac{1}{6} - \lambda_j\lambda_i\right) \mathrm{d}\tau$	0	0	0	$-\frac{2S}{l_k}$	0	0
$\fint_{e_k} \boldsymbol{\omega} \cdot \boldsymbol{t}_k \,\mathrm{d}\tau$	0	0	l_k	0	$5l_k$	0
$\fint_{e_k} \boldsymbol{\omega} \cdot \boldsymbol{t}_k \,(\lambda_j - \lambda_i) \,\mathrm{d}\tau$	0	$\frac{l_j^2 - l_i^2}{2l_k}$	0	$\frac{l_k}{2}$	$-l_k$	0
$\fint_T \boldsymbol{\omega}^{(1)} \,\mathrm{d}x\mathrm{d}y$	$x_i - x_k$	$x_i - x_j$	0	0	0	0
$\fint_T \boldsymbol{\omega}^{(2)} \,\mathrm{d}x\mathrm{d}y$	$y_i - y_k$	$y_i - y_j$	0	0	0	0

Lemma 5.1. *If m cells are concatenated sequentially and every two adjacent cells satisfy $Z_{i,i+1} = 0$, they do not form a vertex-oriented macroelement; see Fig.* 5.2.

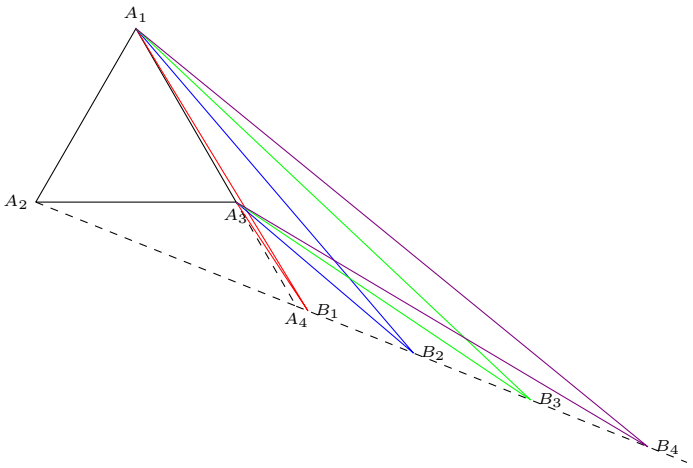

Fig. 5.1. Geometric interpretation of $Z_{12} = 0$.

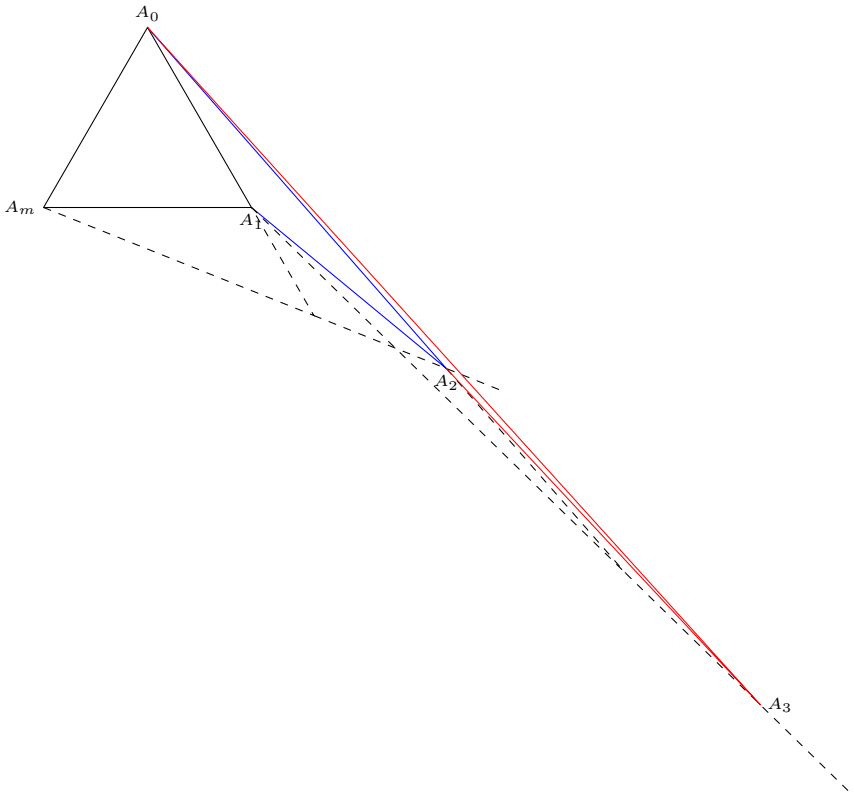

Fig. 5.2. If $Z_{12} = \cdots = Z_{m1} = 0$, the m cells fail to form a vertex-oriented macroelement.

5.2. Verification of the four conditions in Stenberg's technique (Proposition 2.1)

On a macroelement M, we can define $\boldsymbol{V}_{h0,M}^{\mathrm{sBDFM_3}}$ as follows:

$$\boldsymbol{V}_{h0,M}^{\mathrm{sBDFM_3}} := \Big\{ \boldsymbol{v}_h \in \boldsymbol{H}(\mathrm{div}, M) : \boldsymbol{v}_h|_T \in \boldsymbol{P}_3^2(T),\, \forall T \in M;\, \boldsymbol{v}_h \cdot \boldsymbol{n} \text{ and } \fint_e (\boldsymbol{v}_h \cdot \boldsymbol{t})\tau^k \mathrm{d}\tau\, (k=0,1) \text{ are continuous across interior edges and vanish on the edges lying on } \partial M \Big\}. \quad (5.1)$$

Set $M = M_A$ and $M = M_e$ in (5.1) respectively and we have $\boldsymbol{V}_{h0,M_A}^{\mathrm{sBDFM_3}}$ and $\boldsymbol{V}_{h0,M_e}^{\mathrm{sBDFM_3}}$.

Lemma 5.2. *Let $M_A = \cup_{s=1}^m T_s$ $(m \geq 3)$ be a vertex-oriented macroelement as shown in Fig.* 5.3(a). *Then in the following two cases:*

a) m is odd.

b) m is even, and $Z_{12}Z_{23}\cdots Z_{m1} = 0$,

it holds that $\dim(\ker(\mathrm{div}, \boldsymbol{V}_{h0,M_A}^{\mathrm{sBDFM_3}})) = m+1$.

The proof is postponed to Appendix A.2.

Lemma 5.3. *Let $M_A = \cup_{s=1}^m T_s$ $(m \geq 3)$ be a vertex-oriented macroelement as shown in Fig.* 5.3(a). *Then* $\mathrm{div} : \boldsymbol{V}_{h0,M_A}^{\mathrm{sBDFM_3}} \to Q_{h*,M_A}^2$ *is surjective, and*

$$N_{M_A} := \Big\{ q_h \in Q_{h,M_A} : \int_{M_A} \mathrm{div}\, \boldsymbol{v}_h\, q_h = 0,\ \forall\, \boldsymbol{v}_h \in \boldsymbol{V}_{h0,M_A}^{\mathrm{sBDFM_3}} \Big\}$$

is a one-dimensional space containing only constant functions.

Proof. By Lemma 5.2, it holds

$$\begin{aligned} \dim\Big(\mathrm{div}\Big(\boldsymbol{V}_{h0,M_A}^{\mathrm{sBDFM_3}}\Big)\Big) &= \dim\Big(\boldsymbol{V}_{h0,M_A}^{\mathrm{sBDFM_3}}\Big) - \dim\Big(\ker\Big(\mathrm{div}, \boldsymbol{V}_{h0,M_A}^{\mathrm{sBDFM_3}}\Big)\Big) \\ &= (5m+2m) - (m+1) = \dim\big(Q_{h*,M_A}^2\big), \end{aligned}$$

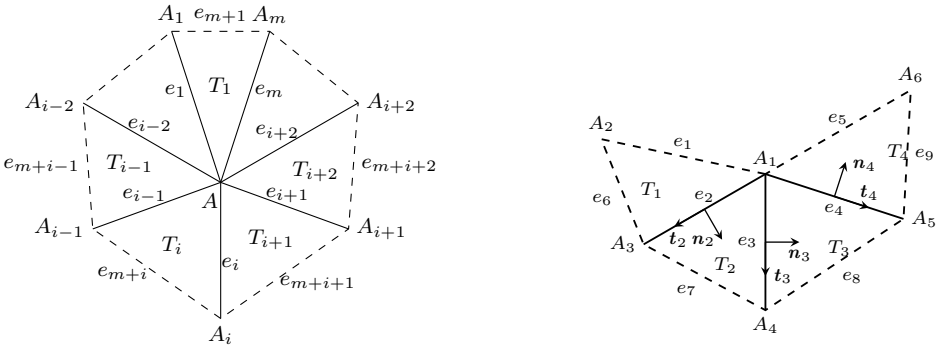

(a) M_A (b) M_{e_3}

Fig. 5.3. Two types of macroelement employed in the inf-sup stability proof of $\mathrm{sBDFM_3} - \mathrm{P_2}$.

which demonstrates that div : $\boldsymbol{V}_{h0,M_A}^{\mathrm{sBDFM}_3} \to Q_{h*,M_A}^2$ is a surjective operator. Then, utilizing the same proof fashion as in Lemma 4.1, we concludes that N_{M_A} is a one-dimensional space containing only constants. □

Lemma 5.4. *Let M_{e_3} be an edge-oriented macroelement (see Fig.* 5.3(b)*) with $Z_{12}Z_{23}Z_{34} \neq 0$. Recall from* (3.12) *that*

$$F(e_3) = S_2 + S_3 + S_2\left(\frac{2R_{23}}{Z_{23}} + \frac{R_{34}}{Z_{34}}\right) + S_3\left(\frac{2R_{23}}{Z_{23}} + \frac{R_{12}}{Z_{12}}\right).$$

If $F(e_3) \neq 0$ then $\dim(\boldsymbol{V}_{h0,M_{e_3}}^{\mathrm{sBDFM}_3}) = 0$. *Moreover,* div : $\boldsymbol{V}_{h0,M_{e_3}}^{\mathrm{sBDFM}_3} \to Q_{h*,M_{e_3}}^2$ *is a surjective operator, and*

$$N_{M_{e_3}} := \left\{ q_h \in Q_{h,M_{e_3}}^2 : \int_{M_{e_3}} \operatorname{div} \boldsymbol{v}_h \, q_h = 0, \ \forall\, \boldsymbol{v}_h \in \boldsymbol{V}_{h0,M_{e_3}}^{\mathrm{sBDFM}_3} \right\}$$

is a one-dimensional space containing only constant functions.

The proof is postponed to Appendix A.3.

Lemma 5.5. *Let $\mathcal{T}_h$ be a triangulations of Ω satisfying Assumptions* 2.1, 2.2, *and* 3.1. *Define the macroelement triangulations $\mathcal{M}_h$ below:*

a) An m-cell vertex-oriented macroelement is defined to the first class of macroelement, if m is odd or m is even and $Z_{12}Z_{23}\cdots Z_{m1} = 0$.

b) For each interior edge e, if it cannot be concluded in any first class of macroelement, then we can get $s(3 \le s \le 5)$ edge-oriented macroelements whose center edge is either e itself or the edges sharing a cell with e, and there must exist some M_{e^*} among the s macroelements such that $F(e^*) \neq 0$, and we define such M_{e^*} to be the second class of macroelement.

Then the $\mathcal{M}_h$ as defined above satisfies the conditions C_1, C_2, C_3 and C_4 in Proposition 2.1.

Proof. The definition of $\mathcal{M}_h$ together with Lemmas 5.3 and 5.4 infers that the conditions C_1 and C_2 holds. Furthermore, since any interior edge $e \in \mathcal{E}_h^i$ belongs to at least one macroelement and no more that seven macroelements(two are the first class macroelements and five the second class macroelements), the condition C_3 is verified. Finally, by Proposition 3.2 and the well-known trace theorem(see, e.g., [4, Theorem 1.6.6]), the condition C_4 also holds. □

Appendix A. Elementary Proof of Three Technical Lemmas

A.1. Proof of Lemma 4.2

Proof. In order to prove $\dim N_{M_A} = 1$ which thus implies N_{M_A} consists of only constant functions on M_A, it is sufficient to show div : $\boldsymbol{V}_{h0,M_A}^{\mathrm{sBDFM}_3} \to Q_{h*,M_A}^2$ is a surjective operator, i.e., $\operatorname{div}(\boldsymbol{V}_{h0,M_A}^{\mathrm{sBDFM}_3}) = Q_{h*,M_A}^2$, which further can be deduced by

$$\dim\ker\left(\operatorname{div}, \boldsymbol{V}_{h0,M_A}^{\mathrm{sBDFM}_3}\right) = 7. \tag{A.1}$$

Hence, it remains to prove (A.1).

To this end, we shall prove firstly

$$\dim\left(\ker\left(\mathrm{div},\, \boldsymbol{W}_{h0,M_A}^{\mathrm{sBDM}_3}\right)\right) = 6, \tag{A.2}$$

where

$$\boldsymbol{W}_{h0,M_A}^{\mathrm{sBDM}_3} := \left\{ \boldsymbol{v}_h \in \boldsymbol{V}_{h0,M_A}^{\mathrm{sBDM}_3} : \fint_e \boldsymbol{v}_h \cdot \boldsymbol{n}_e \,\mathrm{d}\tau = 0,\ e \in \mathcal{E}_h^i(M_A) \right\}.$$

Assume $\boldsymbol{w}_h \in \ker(\mathrm{div}, \boldsymbol{W}_{h0,M_A}^{\mathrm{sBDM}_3})$ with

$$\boldsymbol{w}_h|_T = \sum_{s=1:7} c_{s,T}\boldsymbol{\psi}_{s,T}, \quad \forall T \in M_A.$$

We can establish equations by the continuities on interior edges. For example, considering the continuities on e_1 we reach such relations

$$\begin{cases} c_{1,T_1}\cdot S_1 + c_{2,T_2}\cdot S_2 = 0, \\ c_{3,T_1}\cdot S_1 + c_{4,T_2}\cdot S_2 = 0, \\ c_{5,T_1}\cdot S_1 + c_{6,T_2}\cdot S_2 = 0, \\ -c_{6,T_1} + c_{2,T_2}\cdot\dfrac{S_1+S_2}{S_1} + c_{4,T_2}\cdot\dfrac{5R_{12}}{2S_1} + c_{5,T_2} + c_{6,T_2}\cdot\dfrac{5(S_1+S_2)}{2S_1} = 0, \\ -c_{7,T_1} + c_{4,T_2}\cdot\dfrac{R_{12}}{2S_1} + c_{6,T_2}\cdot\dfrac{S_1+S_2}{2S_1} - c_{7,T_2} = 0. \end{cases}$$

We can build analogous equations based on the continuities on e_2 and e_3.

Denote

$$C_{T_s} \triangleq \begin{bmatrix} c_{1,T_s} & c_{2,T_s} & c_{3,T_s} & c_{4,T_s} & c_{5,T_s} & c_{6,T_s} & c_{7,T_s} \end{bmatrix}, \quad s = 1,2,3.$$

We can form the overall linear system in matrix form

$$\begin{bmatrix} A_{11} & A_{12} & \\ & A_{22} & A_{23} \\ A_{31} & & A_{33} \end{bmatrix} \begin{bmatrix} C_{T_1} \\ C_{T_2} \\ C_{T_3} \end{bmatrix} = \mathbf{0}, \tag{A.3}$$

where

$$A_{ii} = \begin{bmatrix} S_i & 0 & 0 & 0 & 0 & 0 & 0 \\ 0 & 0 & S_i & 0 & 0 & 0 & 0 \\ 0 & 0 & 0 & 0 & S_i & 0 & 0 \\ 0 & 0 & 0 & 0 & 0 & -1 & 0 \\ 0 & 0 & 0 & 0 & 0 & 0 & -1 \end{bmatrix}, \quad i = 1,2,3,$$

$$A_{ij} = \begin{bmatrix} 0 & S_j & 0 & 0 & 0 & 0 & 0 \\ 0 & 0 & 0 & S_j & 0 & 0 & 0 \\ 0 & 0 & 0 & 0 & 0 & S_j & 0 \\ 0 & \dfrac{S_i+S_j}{S_i} & 0 & \dfrac{5R_{ij}}{2S_i} & 1 & \dfrac{5(S_i+S_j)}{2S_i} & 0 \\ 0 & 0 & 0 & \dfrac{R_{ij}}{2S_i} & 0 & \dfrac{S_i+S_j}{2S_i} & -1 \end{bmatrix}, \quad i \neq j.$$

Denote by A the coefficient matrix of (A.3), and after a series of elementary row transformation, A turns out to be

$$\begin{bmatrix} \tilde{A}_1 & \tilde{A}_2 \end{bmatrix}$$

where

$$\tilde{A}_1 = \begin{bmatrix}
S_1 & 0 & 0 & 0 & 0 & 0 & 0 & 0 & S_2 & 0 & 0 & 0 & 0 & 0 & 0 \\
 & S_1 & 0 & 0 & 0 & 0 & 0 & 0 & 0 & 0 & S_2 & 0 & 0 & 0 & S_3 \\
 & & S_1 & 0 & 0 & 0 & 0 & 0 & 0 & 0 & 0 & 0 & 0 & 0 & 0 \\
 & & & S_1 & 0 & 0 & 0 & 0 & 0 & 0 & 0 & 0 & 0 & 0 & 0 \\
 & & & & 1 & \frac{5S_1+5S_3}{2S_3} & 0 & 0 & 0 & 0 & 0 & 0 & 0 & 0 & -\frac{S_1+S_3}{S_1} \\
 & & & & & S_1 & 0 & 0 & 0 & 0 & 0 & 0 & 0 & 0 & 0 \\
 & & & & & & -1 & 0 & 0 & 0 & 0 & 0 & 0 & 0 & 0 \\
 & & & & & & & S_2 & 0 & 0 & 0 & 0 & 0 & 0 & 0 \\
 & & & & & & & & \frac{S_1+S_2}{S_1} & 0 & \frac{5R_{12}}{2S_1} & 1 & \frac{5S_1+5S_2}{2S_1} & 0 & 0 \\
 & & & & & & & & & S_2 & 0 & 0 & 0 & 0 & 0 \\
 & & & & & & & & & & \frac{R_{12}}{2S_1} & 0 & \frac{S_1+S_2}{2S_1} & -1 & 0 \\
 & & & & & & & & & & & S_2 & 0 & 0 & 0 \\
 & & & & & & & & & & & & -1 & 0 & 0 \\
 & & & & & & & & & & & & & -1 & 0 \\
 & & & & & & & & & & & & & & S_1+S_3
\end{bmatrix}$$

$$\tilde{A}_2 = \begin{bmatrix}
0 & 0 & 0 & 0 & 0 & 0 \\
0 & 0 & 0 & 0 & 0 & 0 \\
0 & 0 & 0 & 0 & 0 & 0 \\
0 & S_3 & 0 & 0 & 0 & 0 \\
0 & -\frac{5R_{31}}{2S_1} & 0 & 0 & -1 & 0 \\
0 & 0 & 0 & S_3 & 0 & 0 \\
0 & -\frac{R_{31}}{2S_1} & 0 & -\frac{S_1+S_3}{2S_1} & 0 & -1 \\
S_3 & 0 & 0 & 0 & 0 & 0 \\
0 & 0 & 0 & \frac{S_3}{S_1} & 0 & 0 \\
0 & 0 & S_3 & 0 & 0 & 0 \\
0 & \frac{R_{31}}{2S_1} & 0 & \frac{S_1+S_3}{2S_1} & 0 & 1 \\
0 & 0 & 0 & 0 & S_3 & 0 \\
\frac{S_2+S_3}{S_2} & 0 & \frac{5R_{23}}{2S_2} & 1 & \frac{5S_2+5S_3}{2S_2} & 0 \\
0 & 0 & \frac{R_{23}}{2S_2} & 0 & \frac{S_2+S_3}{2S_2} & -1 \\
S_2+S_3 & \frac{5R_{31}}{2} & \frac{5R_{23}}{2} & \frac{5S_1+5S_3+2S_2}{2} & \frac{5S_2+5S_3+2S_1}{2} & 0
\end{bmatrix}.$$

It reveals that $\operatorname{rank}(A) = 15$, and thus we come to (A.2).

Let $\boldsymbol{v}_h \in \ker(\mathrm{div}, \boldsymbol{V}_{h0,M_A}^{\mathrm{sBDM}_3})$. Considering the continuities of zero-order normal moment across interior edges and using the div theorem in T_1, T_2, T_3, we get

$$l_1 \cdot \fint_{e_1} \boldsymbol{v}_h \cdot \boldsymbol{n}_1 \,\mathrm{d}\tau = l_2 \cdot \fint_{e_2} \boldsymbol{v}_h \cdot \boldsymbol{n}_2 \,\mathrm{d}\tau = l_3 \cdot \fint_{e_3} \boldsymbol{v}_h \cdot \boldsymbol{n}_3 \,\mathrm{d}\tau. \tag{A.4}$$

It implies

$$\fint_{e_1} \boldsymbol{v}_h \cdot \boldsymbol{n}_1 \,\mathrm{d}\tau = 0 \;\Leftrightarrow\; \fint_{e_2} \boldsymbol{v}_h \cdot \boldsymbol{n}_2 \,\mathrm{d}\tau = 0 \;\Leftrightarrow\; \fint_{e_3} \boldsymbol{v}_h \cdot \boldsymbol{n}_3 \,\mathrm{d}\tau = 0.$$

Thus it holds that

$$\begin{aligned}
&\left\{\boldsymbol{v}_h \in \ker\left(\mathrm{div}, \boldsymbol{V}_{h0,M_A}^{\mathrm{sBDM}_3}\right) : \boldsymbol{v}_h \notin \ker\left(\mathrm{div}, \boldsymbol{W}_{h0,M_A}^{\mathrm{sBDM}_3}\right)\right\} \\
=&\left\{\boldsymbol{v}_h \in \ker\left(\mathrm{div}, \boldsymbol{V}_{h0,M_A}^{\mathrm{sBDM}_3}\right) : \fint_e \boldsymbol{v}_h \cdot \boldsymbol{n}_e \,\mathrm{d}s \neq 0,\ e = e_1, e_2, e_3\right\} =: \boldsymbol{Z}_{h0,M_A}^{\mathrm{sBDM}_3}.
\end{aligned}$$

In the remainder, we focus on the space $\boldsymbol{Z}_{h0,M_A}^{\mathrm{sBDM}_3}$ and prove

$$\dim\left(\boldsymbol{Z}_{h0,M_A}^{\mathrm{sBDM}_3}\right) = 1. \tag{A.5}$$

From $\mathrm{Im}(\mathrm{div}, \boldsymbol{V}_{h0,M_A}^{\mathrm{sBDM}_3}) \subset Q_{h*,M_A}^2$, $\dim(Q_{h*,M_A}^2) = 17$ and $\dim(\boldsymbol{V}_{h0,M_A}^{\mathrm{sBDM}_3}) = 24$, it holds that $\dim(\mathrm{Im}(\mathrm{div}, \boldsymbol{V}_{h0,M_A}^{\mathrm{sBDM}_3})) \leqslant 17$ and $\dim(\ker(\mathrm{div}, \boldsymbol{V}_{h0,M_A}^{\mathrm{sBDM}_3})) \geqslant 7$. This fact, together with (A.2), gives $\dim(\boldsymbol{Z}_{h0,M_A}^{\mathrm{sBDM}_3}) \geqslant 1$. Next we show $\dim(\boldsymbol{Z}_{h0,M_A}^{\mathrm{sBDM}_3}) \leqslant 1$.

Assume $\boldsymbol{z}_h \in \boldsymbol{Z}_{h0,M_A}^{\mathrm{sBDM}_3}$ with

$$\boldsymbol{z}_h|_T = \sum_{i=1}^{8} c_{i,T} \boldsymbol{\psi}_{i,T}, \quad \forall\, T \in M_A.$$

From (A.4),

$$\fint_{e_1} \boldsymbol{z}_h \cdot \boldsymbol{n}_1 \,\mathrm{d}s : \fint_{e_2} \boldsymbol{z}_h \cdot \boldsymbol{n}_2 \,\mathrm{d}s : \fint_{e_3} \boldsymbol{z}_h \cdot \boldsymbol{n}_3 \,\mathrm{d}s = \frac{1}{l_1} : \frac{1}{l_2} : \frac{1}{l_3}.$$

It determines a unique relation

$$c_{8,T_1} : c_{8,T_2} : c_{8,T_3} = 1 : 1 : 1,$$

which implies $\dim(\boldsymbol{Z}_{h0,M_A}^{\mathrm{sBDM}_3}) \leqslant 1$, and further (A.5).

The proof of $\dim(\ker(\mathrm{div}, \boldsymbol{V}_{h0,M_A}^{\mathrm{sBDM}_3})) = 7$ concludes with a combination of (A.5) and (A.2). The proof is complete. □

A.2. Proof of Lemma 5.2

Proof. To prove $\dim(\ker(\mathrm{div}, \boldsymbol{V}_{h0,M_A}^{\mathrm{sBDFM}_3})) = m+1$, we shall show $\dim(\ker(\mathrm{div}, \boldsymbol{W}_{h0,M_A}^{\mathrm{sBDFM}_3})) = m$ firstly where

$$\boldsymbol{W}_{h0,M_A}^{\mathrm{sBDFM}_3} := \left\{\boldsymbol{v}_h \in \boldsymbol{V}_{h0,M_A}^{\mathrm{sBDFM}_3} : \fint_e \boldsymbol{v}_h \cdot \boldsymbol{n}_e \,\mathrm{d}\tau = 0,\ e \in \mathcal{E}_h^i(M_A)\right\}.$$

Let $\boldsymbol{w}_h \in \ker(\mathrm{div}, \boldsymbol{W}_{h0,M_A}^{\mathrm{sBDFM}_3})$ with

$$\boldsymbol{w}_h|_T = \sum_{s=1:5} c_{s,T}\boldsymbol{\omega}_{s,T}, \quad \forall\, T \in M_A.$$

Considering the continuity on e_1, we obtain

$$\begin{cases} S_1 \cdot c_{1,T_1} + S_2 \cdot c_{2,T_2} = 0, \\ S_1 \cdot c_{3,T_1} + S_2 \cdot c_{4,T_2} = 0, \\ -S_1 \cdot c_{4,T_1} - Z_{12} \cdot c_{2,T_2} + S_1 \cdot c_{3,T_1} + 2(S_1+S_2) \cdot c_{4,T_2} = 0, \\ -2S_1 \cdot c_{5,T_1} + R_{12} \cdot c_{2,T_2} + (S_1+S_2) \cdot c_{4,T_2} - 2S_1 \cdot c_{5,T_2} = 0. \end{cases}$$

In order to reduce variables, add the third equation by $-5/2$ of the fourth equation, and recall $2Z_{12} + 5R_{12} = 11(S_1+S_2)$, yielding that

$$\begin{aligned} &2S_1 \cdot c_{4,T_1} - 10S_1 \cdot c_{5,T_1} + 11(S_1+S_2) \cdot c_{2,T_2} \\ &\quad - 2S_1 \cdot c_{3,T_2} + (S_1+S_2) \cdot c_{4,T_2} - 10S_1 \cdot c_{5,T_2} = 0. \end{aligned}$$

Travel all the interior edges $e_1, e_2, \cdots, e_m$ and establish the following equations:

$$\begin{bmatrix} A_{11} & A_{12} & & & \\ & A_{22} & A_{23} & & \\ & & \ddots & \ddots & \\ & & & A_{m-1,m-1} & A_{m-1,m} \\ A_{m1} & & & & A_{mm} \end{bmatrix} \begin{bmatrix} \boldsymbol{c}_{T_1} \\ \boldsymbol{c}_{T_2} \\ \vdots \\ \boldsymbol{c}_{T_{m-1}} \\ \boldsymbol{c}_{T_m} \end{bmatrix} = \mathbf{0}, \tag{A.6}$$

where

$$A_{ii} = \begin{bmatrix} S_i & 0 & 0 & 0 & 0 \\ 0 & 0 & S_i & 0 & 0 \\ 0 & 0 & 0 & 2S_i & -10S_i \\ 0 & 0 & 0 & 0 & -2S_i \end{bmatrix}, \quad i = 1, 2, \ldots, m,$$

$$A_{ij} = \begin{bmatrix} 0 & S_j & 0 & 0 & 0 \\ 0 & 0 & 0 & S_j & 0 \\ 0 & 11(S_i+S_j) & -2S_i & S_i+S_j & -10S_i \\ 0 & R_{ij} & 0 & S_i+S_j & -2S_i \end{bmatrix}, \quad i \neq j,$$

and

$$\boldsymbol{c}_{T_s} \triangleq \begin{bmatrix} c_{1,T_s} & c_{2,T_s} & c_{3,T_s} & c_{4,T_s} & c_{5,T_s} \end{bmatrix}^\top, \quad s = 1, 2, \ldots, m,$$

Denote by $Mat \in \mathbb{R}^{4m \times 5m}$ the coefficient matrix of (A.6). If $\mathrm{rank}(Mat) = 4m$, the fundamental system of solutions of (A.6) is m-dimensional, which yields $\dim(\ker(\mathrm{div}, \boldsymbol{W}_{h0,M_A}^{\mathrm{sBDFM}_3})) = m$.

Our next goal is to prove $\mathrm{rank}(Mat) = 4m$. We denote with $r_{i1}, r_{i2}, r_{i3}, r_{i4}$ the rows numbered $4i-3, 4i-2, 4i-1, 4i$ of Mat, and with $c_{i1}, c_{i2}, c_{i3}, c_{i4}, c_{i5}$ the columns numbered $5i-4$, $5i-3, 5i-2, 5i-1, 5i$ of Mat, for $i = 1, 2, \ldots, m$. Assume that there exists a set of constants $\gamma_{i1}, \gamma_{i2}, \gamma_{i3}, \gamma_{i4}, i = 1, 2, \ldots, m$ such that

$$\sum_{i=1}^{m} \gamma_{i1} \cdot r_{i1} + \gamma_{i2} \cdot r_{i2} + \gamma_{i3} \cdot r_{i3} + \gamma_{i4} \cdot r_{i4} = 0,$$

that is,

$$Mat^{\top} * \Gamma \triangleq Mat^{\top} * \begin{bmatrix} \gamma_{11} & \gamma_{12} & \gamma_{13} & \gamma_{14} & \cdots & \gamma_{m1} & \gamma_{m2} & \gamma_{m3} & \gamma_{m4} \end{bmatrix}^{\top} = \mathbf{0}. \tag{A.7}$$

It is easy to see that $\gamma_{i1} = 0$, $i = 1, 2, \ldots, m$.

When m is odd, we have

$$\begin{aligned} &(c_{m5} - c_{15} + c_{25} - \cdots - c_{m-2,5} + cm - 1, 5)^{\top} * \Gamma \\ &= -20S_{m-1} \cdot \gamma_{m-1,3} - 4S_{m-1} \cdot \gamma_{m-1,4} = 0, \end{aligned}$$

from which it holds that

$$5\gamma_{m-1,3} + \gamma_{m-1,4} = 0. \tag{A.8}$$

Recall the $(5m-2)$-th equation of (A.7)

$$S_m \cdot \gamma_{m-1,1} + 11(S_{m-1} + S_m) \cdot \gamma_{m-1,3} + R_{m-1,m} \cdot \gamma_{m-1,4} = 0,$$

and combine it with (A.8), we get $11(S_{m-1} + S_m) = 5R_{m-1,m}$, and thus $Z_{m-1,m} = 0$.

By a same fashion, we obtain $Z_{12} = Z_{23} = \cdots = Z_{m-1,m} = Z_{m1}$. By Lemma 5.1 we know that $T_1 \cup T_2 \cup \cdots \cup T_m$ fail to form a closed vertex-oriented macroelement, which contradicts the beginning assumption. Therefore, we have

$$\gamma_{ij} = 0, \quad i = 1, 2, \ldots, m, \quad j = 1, 2, 3, 4. \tag{A.9}$$

When m is even, and $Z_{12}Z_{23}\cdots Z_{m1} = 0$, then we assume $Z_{m1} = 0$, i.e., $11(S_m + S_1) = 5R_{m1}$. From the second equation of (A.7), it follows that $5\gamma_{m,3} + \gamma_{m,4} = 0$, Bringing it into the fifth equation of (A.7), we have $5\gamma_{13} + \gamma_{14} = 0$, which combined with the seventh equation of (A.7) yields $11(S_1 + S_2) = 5R_{12}$, i.e., $Z_{12} = 0$. Analogously, we can prove $Z_{12} = Z_{23} = \cdots = Z_{m-1,m} = Z_{m1}$ and ultimately (A.9) is obtained as well.

The above analysis show that the homogeneous linear system (A.7) has only zero solution, thus $\operatorname{rank}(Mat) = 4m$, and further the solution space of (A.6) is m-dimensional, which leads to $\dim(\ker(\operatorname{div}, \boldsymbol{W}_{h0,M_A}^{\mathrm{sBDFM}_3})) = m$.

Finally we shall prove $\dim(\ker(\operatorname{div}, \boldsymbol{V}_{h0,M_A}^{\mathrm{sBDFM}_3})) = m + 1$. Let $\boldsymbol{w}_h \in \ker(\operatorname{div}, \boldsymbol{V}_{h0,M_A}^{\mathrm{sBDFM}_3})$. The divergence theorem gives

$$\int_{e_1} \boldsymbol{v}_h \cdot \boldsymbol{n}_1 = \int_{e_2} \boldsymbol{v}_h \cdot \boldsymbol{n}_2 = \cdots = \int_{e_m} \boldsymbol{v}_h \cdot \boldsymbol{n}_m.$$

Assume there exists some $\boldsymbol{v}_h^* \in \ker(\operatorname{div}, \boldsymbol{V}_{h0,M_A}^{\mathrm{sBDFM}_3})$ such that $\int_{e_i} \boldsymbol{v}_h^* \cdot \boldsymbol{n}_i \, \mathrm{d}s = 1$ for $i = 1, 2, \ldots, m$. Then for any $\boldsymbol{v}_h \in \ker(\operatorname{div}, \boldsymbol{V}_{h0,M_A}^{\mathrm{sBDFM}_3})$, there exists α such that

$$\boldsymbol{v}_h = \alpha \boldsymbol{v}_h^* + \boldsymbol{w}_h, \quad \boldsymbol{w}_h \in \ker\left(\operatorname{div}, \boldsymbol{W}_{h0,M_A}^{\mathrm{sBDFM}_3}\right),$$

which shows that

$$\ker\left(\operatorname{div}, \boldsymbol{V}_{h0,M_A}^{\mathrm{sBDFM}_3}\right) = \ker\left(\operatorname{div}, \boldsymbol{V}_{h0,M_A}^{\mathrm{sBDFM}_3}\right) \oplus \operatorname{span}\{\boldsymbol{v}_h^*\}.$$

On the other hand, we can deduce that

$$\dim\left(\ker\left(\operatorname{div}, \boldsymbol{V}_{h0,M_A}^{\mathrm{sBDFM}_3}\right)\right) = \dim\left(\boldsymbol{V}_{h0,M_A}^{\mathrm{sBDFM}_3}\right) - \dim\left(\operatorname{div}\left(\boldsymbol{V}_{h0,M_A}^{\mathrm{sBDFM}_3}\right)\right)$$

$$\geq \dim\left(\boldsymbol{V}_{h0,M_A}^{\mathrm{sBDFM}_3}\right) - \dim\left(Q_{h*,M_A}^2\right) = m+1,$$

suggesting the existence of $\boldsymbol{v}_h^*$. Therefore, we come to $\dim(\ker(\mathrm{div}, \boldsymbol{V}_{h0,M_A}^{\mathrm{sBDFM}_3})) = m+1$. The proof is complete. □

A.3. Proof of Lemma 5.4

Proof. Assume $\boldsymbol{v}_h \in \ker(\mathrm{div}, \boldsymbol{V}_{h0,M_{e_3}}^{\mathrm{sBDFM}_3})$, with

$$\boldsymbol{v}_h = \sum_{s=1:6} c_{s,T}\boldsymbol{\omega}_{s,T}, \quad \forall T \in M_{e_3}.$$

Firstly, using the divergence theorem on T_1 and T_4 we have

$$\boldsymbol{v}_h|_{T_1} \in \mathrm{span}\{\boldsymbol{\omega}_{1,T_1}\}, \quad \boldsymbol{v}_h|_{T_4} \in \mathrm{span}\{\boldsymbol{\omega}_{2,T_4}\}.$$

Further, by Table 5.1,

$$\boldsymbol{v}_h|_{T_2} \in \mathrm{span}\{\boldsymbol{\omega}_{1,T_2}, \boldsymbol{\omega}_{2,T_2}, \boldsymbol{\omega}_{3,T_2}, \boldsymbol{\omega}_{5,T_2}\}, \quad \boldsymbol{v}_h|_{T_3} \in \mathrm{span}\{\boldsymbol{\omega}_{1,T_3}, \boldsymbol{\omega}_{2,T_3}, \boldsymbol{\omega}_{4,T_3}, \boldsymbol{\omega}_{5,T_3}\}.$$

Now, by continuities on interior edges e_2, e_3, e_4 we can establish the following linear system:

$$\begin{bmatrix}
S_1 & S_2 & 0 & 0 & 0 & & & & & \\
0 & 11(S_1+S_2) & -10S_1 & -2S_1 & 0 & & & & & \\
0 & R_{12} & -2S_1 & 0 & 0 & & & & & \\
 & & 0 & 0 & S_2 & S_3 & 0 & 0 & 0 & \\
 & & 0 & S_2 & 0 & 0 & S_3 & 0 & 0 & \\
 & & -10S_2 & 0 & 0 & 11(S_2+S_3) & S_2+S_3 & -10S_2 & 0 & \\
 & & -2S_2 & 0 & 0 & R_{23} & S_2+S_3 & -2S_2 & 0 & \\
 & & & & & 0 & 0 & 0 & S_3 & S_4 \\
 & & & & & 0 & 2S_3 & -10S_3 & 0 & 11(S_3+S_4) \\
 & & & & & 0 & 0 & -2S_3 & 0 & R_{34}
\end{bmatrix}
\begin{bmatrix}
c_{1,T_1} \\ c_{2,T_2} \\ c_{5,T_2} \\ c_{3,T_2} \\ c_{1,T_2} \\ c_{2,T_3} \\ c_{4,T_3} \\ c_{5,T_3} \\ c_{1,T_3} \\ c_{2,T_4}
\end{bmatrix} = \mathbf{0}. \quad \text{(A.10)}$$

From the first three equations of (A.10), we know that

$$c_{2,T_2} = -\frac{S_1}{S_2}c_{1,T_1}, \quad c_{5,T_2} = -\frac{R_{12}}{2S_2}c_{1,T_1}, \quad c_{3,T_2} = -\frac{Z_{12}}{S_2}c_{1,T_1}. \quad \text{(A.11)}$$

Analogously, from the rearmost three equations in (A.10) we have

$$c_{1,T_3} = -\frac{S_4}{S_3}c_{2,T_4}, \quad c_{5,T_3} = \frac{R_{34}}{2S_3}c_{2,T_4}, \quad c_{4,T_3} = -\frac{Z_{34}}{S_3}c_{2,T_4}. \quad \text{(A.12)}$$

Substituting the relations (A.11) and (A.12) into the middle four lines of the Eq. (A.10), a smaller linear system equivalent to the original system (A.10) is obtained

$$\begin{bmatrix}
Z_{12} & 0 & 0 & Z_{34} \\
0 & S_2 & S_3 & 0 \\
5R_{12} & 0 & 11(S_2+S_3) & -\dfrac{(S_2+S_3)Z_{34}+5S_2R_{34}}{S_3} \\
R_{12} & 0 & R_{23} & -\dfrac{(S_2+S_3)Z_{34}+S_2R_{34}}{S_3}
\end{bmatrix}
\begin{bmatrix}
c_{1,T_1} \\ c_{1,T_2} \\ c_{2,T_3} \\ c_{2,T_4}
\end{bmatrix} = \begin{bmatrix} 0 \\ 0 \\ 0 \\ 0 \end{bmatrix}.$$

After elementary row transformations, the above equations can be further converted to

$$\begin{bmatrix} Z_{12} & 0 & 0 & Z_{34} \\ 0 & S_2 & S_3 & 0 \\ 0 & 0 & Z_{23} & -\dfrac{2(S_2+S_3)Z_{34}}{S_3} \\ 0 & 0 & 0 & S_2\left(1+\dfrac{2R_{23}}{Z_{23}}+\dfrac{R_{34}}{Z_{34}}\right)+S_3\left(1+\dfrac{2R_{23}}{Z_{23}}+\dfrac{R_{12}}{Z_{12}}\right) \end{bmatrix} \begin{bmatrix} c_{1,T_1} \\ c_{1,T_2} \\ c_{2,T_3} \\ c_{2,T_4} \end{bmatrix} = \begin{bmatrix} 0 \\ 0 \\ 0 \\ 0 \end{bmatrix}. \quad \text{(A.13)}$$

If

$$S_2\left(1+\frac{2R_{23}}{Z_{23}}+\frac{R_{34}}{Z_{34}}\right)+S_3\left(1+\frac{2R_{23}}{Z_{23}}+\frac{R_{12}}{Z_{12}}\right)\neq 0,$$

then (A.13) has unique solution, and further $\dim(\ker(\mathrm{div}, \boldsymbol{V}_{h0,M_{e_3}}^{\mathrm{sBDFM_3}})) = 0$.

Moreover,

$$\begin{aligned} \dim\left(\mathrm{div}\left(\boldsymbol{V}_{h0,M_{e_3}}^{\mathrm{sBDFM_3}}\right)\right) &= \dim\left(\boldsymbol{V}_{h0,M_{e_3}}^{\mathrm{sBDFM_3}}\right) - \dim\left(\ker\left(\mathrm{div}, \boldsymbol{V}_{h0,M_{e_3}}^{\mathrm{sBDFM_3}}\right)\right) \\ &= 23 - 0 = \dim\left(Q_{h*,M_{e_3}}^2\right), \end{aligned}$$

which implies that $\mathrm{div} : \boldsymbol{V}_{h0,M_{e_3}}^{\mathrm{sBDFM_3}} \to Q_{h*,M_{e_3}}^2$ is surjective.

Finally, a same proof fashion as in Lemma 4.1 concludes that $N_{M_{e_3}}$ is a one-dimensional space containing only constants. □

Acknowledgements. This paper is supported partially by the Strategic Priority Research Program of Chinese Academy of Sciences (Grant No. XDB0640000) and by the National Natural Science Foundation of China (Grant No. 12271512). The work of the first author is also supported in part by the Research Start-up Fund of Shanxi University (Grant No. 109541077).

References

[1] F. Auricchio, L.B. Veiga, C. Lovadina, and A. Reali, The importance of the exact satisfaction of the incompressibility constraint in nonlinear elasticity: Mixed fems versus nurbs-based approximations, *Comput. Methods Appl. Mech. Engrg.*, **199** (2010), 314–323.

[2] F. Auricchio, L.B. Veiga, C. Lovadina, A. Reali, R.L. Taylor, and P. Wriggers, Approximation of incompressible large deformation elastic problems: Some unresolved issues, *Comput. Mech.*, **52** (2013), 1153–1167.

[3] D. Boffi, F. Brezzi, and M. Fortin, *Mixed Finite Element Methods and Applications*, Springer, 2013.

[4] S.C. Brenner and L.R. Scott, *The Mathematical Theory of Finite Element Methods*, Springer, 2008.

[5] B. Cockburn, G. Kanschat, and D. Schötzau, A note on discontinuous Galerkin divergence-free solutions of the Navier-Stokes equations, *J. Sci. Comput.*, **31** (2007), 61–73.

[6] R.S. Falk and M. Neilan, Stokes complexes and the construction of stable finite elements with pointwise mass conservation, *SIAM J. Numer. Anal.*, **51**:2 (2013), 1308–1326.

[7] L.P. Franca and T.J.R. Hughes, Two classes of mixed finite element methods, *Comput. Methods Appl. Mech. Engrg.*, **69**:1 (1988), 89–129.

[8] K.J. Galvin, A. Linke, L.G. Rebholz, and N.E. Wilson, Stabilizing poor mass conservation in incompressible flow problems with large irrotational forcing and application to thermal convection, *Comput. Methods Appl. Mech. Engrg.*, **237-240** (2012), 166–176.

[9] J. Guzmán and M. Neilan, A family of nonconforming elements for the Brinkman problem, *IMA J. Numer. Anal.*, **32**:4 (2012), 1484–1508.

[10] J. Guzmán and M. Neilan, Conforming and divergence-free Stokes elements on general triangular meshes, *Math. Comput.*, **83**:285 (2014), 15–36.

[11] R. Hiptmair, L. Li, S. Mao, and W. Zheng, A fully divergence-free finite element method for magnetohydrodynamic equations, *Math. Models Methods Appl. Sci.*, **28** (2018), 1–37.

[12] K. Hu, Y. Ma, and J. Xu, Stable finite element methods preserving $\nabla \cdot \mathbf{B} = 0$ exactly for MHD models, *Numer. Math.*, **135**:2 (2017), 371–396.

[13] K. Hu and J. Xu, Structure-preserving finite element methods for stationary MHD models, *Math. Comput.*, **88**:316 (2019), 553–581.

[14] V. John, A. Linke, C. Merdon, M. Neilan, and L.G. Rebholz, On the divergence constraint in mixed finite element methods for incompressible flows, *SIAM Rev.*, **59**:3 (2017), 492–544.

[15] G. Kanschat and N. Sharma, Divergence-conforming discontinuous Galerkin methods and C^0 interior penalty methods, *SIAM J. Numer. Anal.*, **52**:4 (2014), 1822–1842.

[16] A. Linke, A divergence-free velocity reconstruction for incompressible flows, *C. R. Math.*, **350**:17-18 (2012), 837–840.

[17] A. Linke, G. Matthies, and L. Tobiska, Robust arbitrary order mixed finite element methods for the incompressible Stokes equations with pressure independent velocity errors, *ESAIM Math. Model. Numer. Anal.*, **50**:1 (2016), 289–309.

[18] W. Liu and S. Zhang, A lowest-degree conservative finite element scheme for incompressible Stokes problems on general triangulations, *J. Sci. Comput.*, **93** (2022), 28.

[19] K.A. Mardal, X.C. Tai, and R. Winther, A robust finite element method for Darcy-Stokes flow, *SIAM J. Numer. Anal.*, **40**:5 (2002), 1605–1631.

[20] L.R. Scott and M. Vogelius, Norm estimates for a maximal right inverse of the divergence operator in spaces of piecewise polynomials, *ESAIM Math. Model. Numer. Anal.*, **19**:1 (1985), 111–143.

[21] R. Stenberg, A technique for analysing finite element methods for viscous incompressible flow, *Int. J. Numer. Methods Fluids*, **11**:6 (1990), 935–948.

[22] X.C. Tai and R. Winther, A discrete de Rham complex with enhanced smoothness, *Calcolo*, **43**:4 (2006), 287–306.

[23] E. Vanderzee, A.N. Hirani, D. Guoy, and E.A. Ramos, Well-centered triangulation, *SIAM J. Sci. Comput.*, **31**:6 (2010), 4497–4523.

[24] J. Wang, Y. Wang, and X. Ye, A robust numerical method for Stokes equations based on divergence-free $H(\mathrm{div})$ finite element methods, *SIAM J. Sci. Comput.*, **31**:4 (2009), 2784–2802.

[25] J. Wang and X. Ye, New finite element methods in computational fluid dynamics by $H(\mathrm{div})$ elements, *SIAM J. Numer. Anal.*, **45**:3 (2007), 1269–1286.

[26] M. Wang, The generalized Korn inequality on nonconforming finite element spaces, *Chinese J. Numer. Math. Appl.*, **16**:2 (1994), 91–96.

[27] X. Xie, J. Xu, and G. Xue, Uniformly stable finite element methods for Darcy-Stokes-Brinkman models, *J. Comput. Math.*, **26**:3 (2008), 437–455.

[28] Y. Yue, H. Chen, and S. Zhang, Lower and upper bounds for Stokes eigenvalues, *Calcolo*, **61** (2024), 48.

[29] H. Zeng, C.-S. Zhang, and S. Zhang, A low-degree strictly conservative finite element method for incompressible flows, *SMAI J. Comput. Math.*, **8** (2022), 225–248.